Pisa, 04 aprile 2013

CONSIGLIO NAZIONALE DELLE RICERCHE

Istituto Nazionale di Ottica

Laboratorio Irraggiamento Laser Intensi – ILIL
http://ilil.ino.it

Internal Report

Title:
Laser-plasma acceleration at LNF-Frascati – a selection from the LNF internal report contributions on the subject from 2003 to 2011

2003-2011 – Laser plasma acceleration programme at LNF-INFN
A collection of the LNF-INFN yearly reports

Abstract: Since 2003, the ILIL group has co-promoted the development of the laser-plasma acceleration programme at LNF-INFN, Frascati. Regular updates of the activity, with special attention to the FLAME laser installation development, were included in the reports of LNF-INFN. From 2003 to 2006 the activity is briefly mentioned in the corresponding reports, with reference to the FLAME laser or the PLASMONX project. Starting in 2007, dedicated chapters were prepared, with contribution from the Pisa laser-plasma (INO-ILIL) group on the laser and laser-plasma part. These contents are herewith collected as an account of the ILIL activity at LNF-INFN during the past years.

2003

Extracts from Alesini *et al.*,"SPARC", LNF Annual Activity Report 2003, pp. 242

"Beams with the features anticipated in the SPARC project are also of strong interest for experiments in other cutting edge fields. The SPARC injector may allow investigations into the physics of ultra-short beams, plasma wave-based acceleration, and production of Compton back-scattered X-rays (PLASMON/MAMBO activities)."

2004

Extracts from Alesini *et al.*,"SPARC", LNF Annual Activity Report 2004, pp. 226

"Beams with the features anticipated in the SPARC project are also of strong interest for experiments into other cutting edge fields. The SPARC injector may allow investigations into the physics of ultra-short beams, plasma wave-based acceleration, and production of X-ray Compton back-scattering (PLASMON/MAMBO activities)."

2005

Extracts from Calvetti M., "FOREWORD - Laboratori Nazionali di Frascati – Frascati National Laboratories (LNF): Present and Future", LNF Annual Activity Report 2005, pp. VII-VIII

"A very intense LASER, able to produce 200 TW of 0.8 micron wave length for 10 fs (the Frascati Laser for Acceleration and Multidisciplinary Experiments, FLAME) is being assembled nearby the SPARC linac. The possibility to accelerate a bunch of electrons in the plasma waves produced by the light in a gaseous target will be explored."

"The FLAME laser will be operational by the end of the year 2008."

2006

Extracts from Calvetti M. "FOREWORD - Laboratori Nazionali di Frascati – Frascati National Laboratories (LNF): Present and Future", LNF Annual Activity Report 2006, pp.VII

"A very intense LASER, able to produce 200 TW of 0.8 micron wave length for 10 fs (the Frascati Laser for Acceleration and Multidisciplinary Experiments, FLAME) is being assembled nearby the SPARC linac. The possibility to accelerate a bunch of electrons in the plasma waves produced by the light in a gaseous target will be explored.

"The FLAME laser will be operational by the end of the year 2008."

Extracts from Alesini *et al.*, "SPARC", LNF Annual Activity Report 2006, pp. 252

"The SPARC injector will allow also investigations into the physics of ultra-short beams, plasma wave-based acceleration, and production of X-ray Compton back-scattering as reported in the PLASMON activity section."

From LNF-INFN report 2007

PLASMON-X

C. Benedetti, V. Lucarini, P. Londrillo, S. Rambaldi, A. Sgattoni, G. Servizi,
G. Turchetti, F. Zanlungo **Sez. INFN Bologna**
R. Bonifacio, M. Castellano, A. Clozza, L. Cultrera, G. Di Pirro, A. Drago, M. Esposito,
M. Ferrario, D. Filippetto, A. Gallo, G. Gatti, P. Gaudio, A. Ghigo, A. La Monaca,
M. Migliorati, D. Nanni, E. Pace, L. Palumbo, M. Richetta, C. Sanelli, F. Tazzioli,
A. Tenore, F. Terra, S. Tomassini, C. Vaccarezza, C. Vicario - **Lab. Naz. di Frascati**
L. Calabretta, C. Cavallaro, L. Giuffrida, R. Miracoli, L. Torrisi - **Lab. Naz. del Sud**
A. L. Bacci, F. Broggi, M.M.Cola, G. D'angelo, C De Martinis, A. Fazzi,
A. S. Giulini Castiglioni, C. Maroli, M. Passoni, V. Petrillo, N. Piovella,
A. Pola, R. Pozzoli, M. Rome', A. R. Rossi, L. Serafini, P. Tomassini - **Sez. INFN Milano**
A. Galassi, D. Batani, G. Lucchini, R. Jafer, R. Redaelli,
R. Benocci, T. Desai - **Sez. INFN Milano Bicocca**
U. De Angelis, S. De Nicola, R. Fedele, G. Fiore, C. Stornaiolo - **Sez. INFN Napoli**
S. Betti, C.A. Cecchetti, A. Giulietti, D. Giulietti, A.Gamucci, L.A. Gizzi,
P. Koester, L. Labate, T. Levato, A. Macchi, M. Vaselli **Sez. INFN & CNR Pisa**

1 Aim of the experiment

The two main goals of the PLASMON-X project are the development of an innovative, high-gradient, laser-driven acceleration technique and the set up of a tuneable, hard X/γ-ray source, based upon Thomson Scattering (TS) of optical photons by energetic electrons. The laser driven acceleration will be investigated both in the self-injection scheme based upon the Laser Wake Field Acceleration (LWFA) and in the external injection scheme, using the electron bunches generated by the SPARC linac. Both experiments require very high power, ultra-short laser pulses in combination with very bright and short electron bunches.

Our programme follows the impressive progress in the field of laser-driven acceleration that has been achieved in the very recent years thanks to the advent of the ultra-short pulse lasers based upon the Chirped Pulse Amplification (CPA) technique [3]. In fact, CPA has allowed few joules, femtosecond pulses to be produced and used at a repetition rate of 10 Hz. Recently, very encouraging results have been achieved concerning the energy and the quality of the electron bunches produced by LWFA [4, 5, 6, 7]. Electrons with energies above 100 MeV and with an high degree of monochromaticity have been experimentally obtained and reproduced in many laboratories worldwide, while in some cases electron top energies above 1 GeV have been reached [8]. These experiments strongly suggest the possibility of setting up a prototype of a fully optical electron accelerator, provided that both laser and plasma performances are experimentally controlled with an high accuracy. With such an apparatus one would be also capable of accelerating externally generated electron bunches which, once produced by a suitable source, could be injected into a laser-generated plasma, where they could experience an high gradient accelerating field capable of significantly increasing their energy. In our case, the external source of electron bunches will be either a conventional Radio-Frequency (RF) accelerator or a laser-plasma injector, i.e. a second laser-driven electron accelerator. In view of this, the recent PLASMON-X project activity has also been devoted to performing basic experiments [9, 10, 11, 12, 13] aimed at investigating the possibility of adopting a laser-driven accelerator also as an electron photo-injector.

2 Group activity: experimental

2.1 Laser set up

During 2007, the lased design was completed and construction of the system started at Amplitude Technologies (Fr). The image of Figure 1 shows the front-end of the laser assembled at the Amplitude factory. The FLAME laser is a CPA system that will deliver < 20 fs, 800 nm, up to 300 TW, laser pulses with a 10 Hz repetition rate. The system features a high, sub-ns contrast ratio ($> 10^{10}$) and has a fully remotely controlled operation mode. In view of the above discussed requirements for prototyping of a laser-based electron photo-injector, the laser system will provide shot by shot monitoring of both temporal and spatial properties of the laser pulse. Spatial characterization will be performed both in the near and in the far field, using an equivalent plane monitor. Temporal characterization will be performed using two kinds of diagnostics. The first one will operate on a multiple-shot base while the second will operate in a single-shot regime. The multiple-shot diagnostics will offer the advantage of a better performance in view of a fine tuning of the laser parameters during setup. A third order autocorrelator will instead be used to monitor the contrast ratio. Also an interferometric second order autocorrelator will be set up to monitor the oscillator behaviour. The shot by shot performance of the laser system will be monitored using a second order single-shot autocorrelator.

Figure 1: *Front end of the FLAME laser system assembled for testing at the factory. The front end includes the advanced system for contrast enhancement and DAZZLER-MAZZLER combination for bandwidth and pulse duration optimisation.*

As anticipated above, synchronisation of the FLAME laser system with the LINAC will be required. In the existing set-up, the CPA laser driving the LINAC photoinjector is already synchronized with an external radiofrequency by changing dynamically the length of the oscillator cavity. The final result is a jitter between the radiofrequency and the laser pulse of less than 1 ps. This jitter is still much higher than that required in the case of acceleration of externally injected electrons. This issue is presently under investigation within the Comm.V project named FAST (Femtosecond Active Sync and Timing) and a preliminary characterisation of the sub-picosecond jitter of the LINAC bunches has already been carried out. Based on this characterisation, a dedicated synchronization system is being studied which is based upon an electro-optics approach [25].

2.2 The FLAME Laboratory

During 2007, the design of the basic layout of the FLAME installation at LNF that will allow execution of the PLASMON-X scientific programme was completed and the construction of the building was carried out. Figure 2 shows the top and side view of the FLAME laboratory with the layout of the laser and of the laser beam transport line up to the bunker connection conduits.

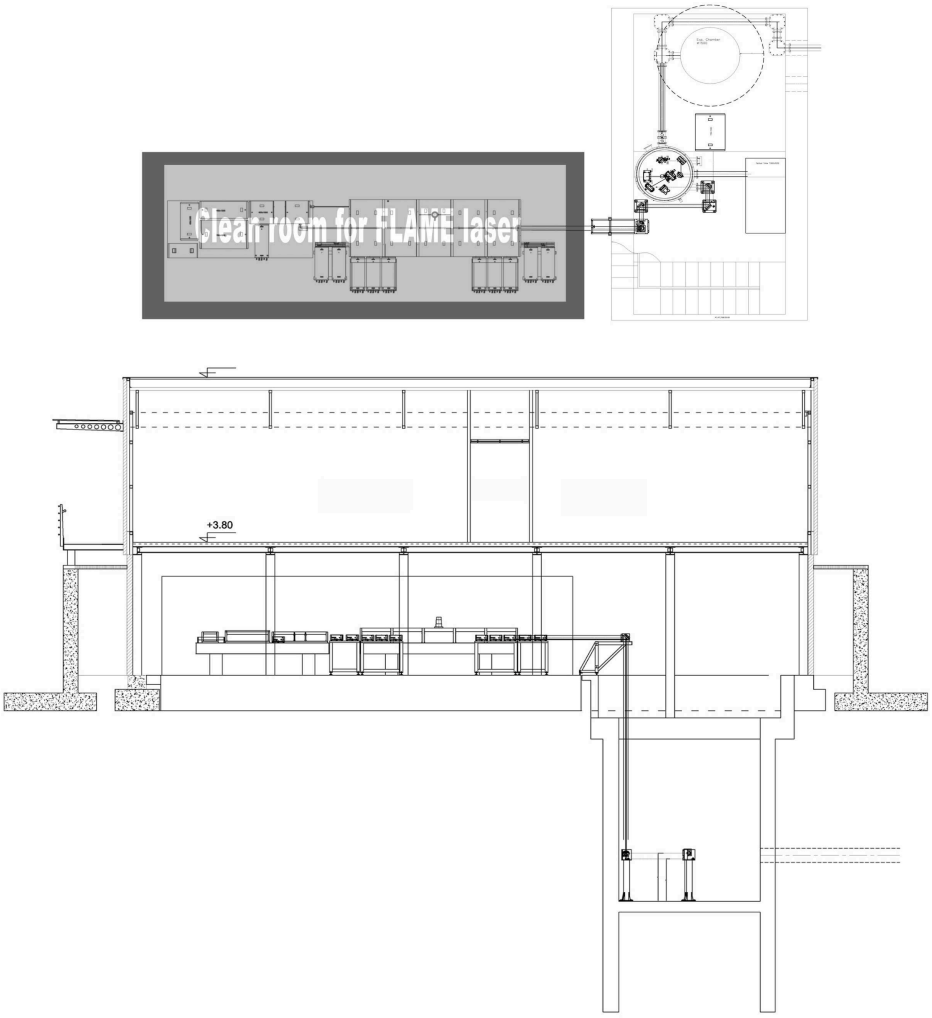

Figure 2: *Up (on top) and side (on bottom) view of the FLAME laboratory with the layout of the laser and of the laser beam transport line up to the bunker connection conduits.*

The 10 Hz, 300 TW TiSa laser system and the 10 Hz, 150 MeV SPARC [1, 2] linear accelerator are now well into the construction phase and additional R&D on ultra-fast electron-photon synchronization is being planned. The set of experiments identified for the first phase of operation of the installation include laser-driven acceleration of self-injected as well as externally injected electron bunches, TS aimed at the production of tunable, hard X-rays for bio-medical applications. All these experiments have now been under extensive modelling and test experiments are already in progress at collaborating small-scale laboratories. A significant part of the Plasmon-X

experimental activity has in fact been carried out at LASERLAB laser facilities, including CLF at RAL (UK) and SLIC at CEA-Saclay. In addition, an intense R&D activity on laser driven acceleration was carried out in collaboration with the INFN section of Pisa at the CNR-IPCF laboratory in Pisa, where a moderate laser power installation exists. Here we briefly describe the main streams on which group activity has been prevalently focused in 2007, and summarize recent results on the modelling of the experiments.

2.3 Laser-driven acceleration: the precursor experiment

The laser-driven electron acceleration experiment which has been set up at the CNR (IPCF) Laboratory in Pisa, in collaboration with Sez. Pisa INFN, during 2007 and early 2008 is based upon a Ti:Sa laser system generating a main pulse of 67 fs duration FWHM at the repetition rate of 10 Hz. Within the PLASMON-X activity, a fraction (10 %) of the existing 67 fs laser pulse was further amplified by a 6-pass amplifier pumped by a frequency doubled Nd:YAG laser delivering 1 J pulses pumping a 2-cm diameter TiSa crystal. The output is further expanded to a 33 mm diameter beam and compressed by a two-grating compressor placed under vacuum. The pulse is compressed to a minimum pulse duration of 67 fs and is then transported under vacuum into the target chamber via two beam steering, motorised turning mirrors, placed in two separate small vacuum chambers. A diagram of the back-end of the laser system, showing a top view of the vacuum compressor and the beam steering mirrors is shown in Figure 3.

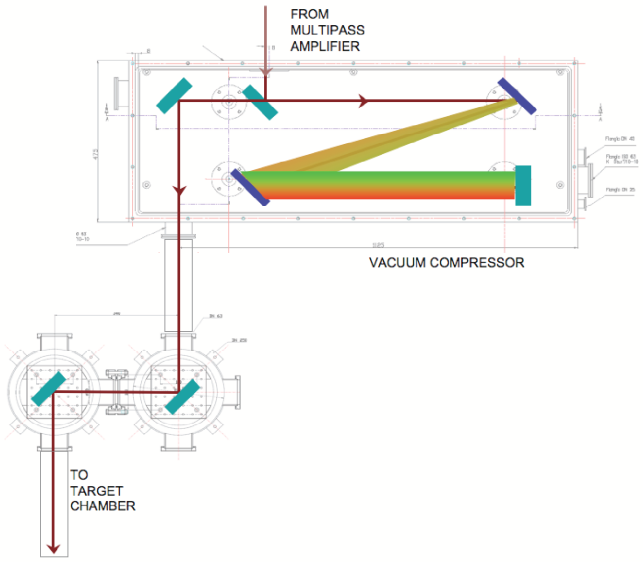

Figure 3: *Schematic layout of the last components of the laser system, including the vacuum compressor and the beam steering mirrors.*

The temporal and spatial properties of the femtosecond pulses have been characterised in detail using custom developed second-order autocorrelator. The contrast of the laser pulse, i.e. the ratio between the peak power and the low intensity pedestal originating both from prepulses and from amplified spontaneous emission (ASE) was measured with a third-order cross-correlator (SEQUOIA). According to the characteristion measurements, the FWHM focal spot on target using an f/6 numerical aperture is approx. 10 μm. Considering the pulse length of 67 fs and an energy of 120 mJ we find that the peak intensity on the target can exceed 10^{18} W/cm^2 required for laser-plasma acceleration.

3 Group activity: theoretical modelling

In this section we describe the theoretical activity which has been developed concerning the production and acceleration of high quality electron beams. The key parameters here are energy gain and energy spread, and various ways of reducing the energy spread are being investigated.

3.1 Self injection in Laser Wake Field

In the scheme proposed in [21], the production of high-quality electron beams in the LWFA regime is achieved via activation of a controlled longitudinal non-linear wave-breaking. The latter is induced by a suitably chosen electron density profile characterized by a downward step-like feature along the laser propagation direction. The initial plasma density profile consists of a smooth rising edge and of a first plateau where an high amplitude plasma wave is excited. Next, a density downramp makes a transition to a second, lower density plateau. According to both 1D analytical results and 2.5D numerical simulations, a partial break of the wave crests at the transition (downramp) capable of injecting electrons with the appropriate phase with the plasma wave excited in the second plateau (accelerating region) might occur. As the plasma density decreases in the direction of the pulse propagation, the wave number increases with time. This results in a decrease of the phase velocity and in a breaking of the wave at the interface between the two uniform density regions, even if the wave initial amplitude is below the nonlinear wave-breaking threshold. As a result of the wave breaking which occurs at the interface between the two density regions, fast electrons from the wave crest are trapped by the wave and accelerated into the lower density region where the wake field remains regular. PIC simulations indeed show that this approach successfully generates mono-energetic electron bunches [22]. Figure 4 (left) shows the energy spectrum of the electrons produced by such an acceleration scheme as obtained by PIC simulations [22].

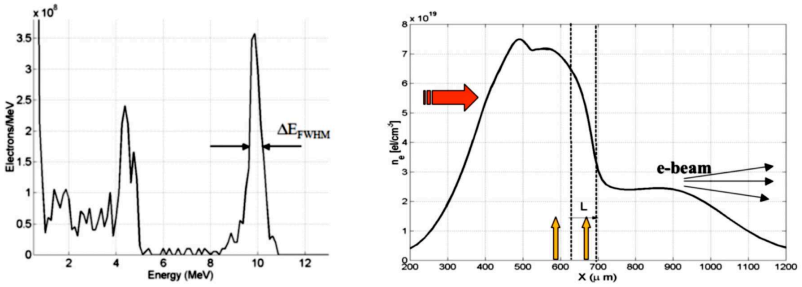

Figure 4: *Energy spectrum (left) of the accelerated electrons in a pre-formed plasma with a sharp density depletion (shown on right). The spectrum is obtained with 2-dimensional hydrodynamic simulations of laser explosion of a two-foil target as shown by the yellow arrows. The red arrow indicates the direction of propagation of the laser pulse.*

In the simulations, the electron density profile consisted of a smooth vacuum-plasma transition followed by a first density plateau ($n_e = 2.1 \times 10^{19}$ cm^{-3}). Then, an abrupt density decrease on a scale length of $L = 60$ μm leads to a second density plateau ($n_e = 1.1 \times 10^{19}$ cm^{-3}), as shown in Figure 4 (right). In the simulation, the laser pulse is 1 μm wavelength and has a Gaussian envelope (waist $w = 20$ μm, time duration $\tau_{\mathrm{FWHM}} = 17$ fs) with an intensity of $I = 2.5 \times 10^{18}$ W/cm^2. From the plot of Figure 4 (left) we can see that the electrons with energy above 7 MeV represent a bunch of $N_e \approx 10^8$ particles with energy $E \approx 10MeV$ and energy spread of less than 5 %, while the transverse and longitudinal spatial bunch extent are 1 μm and 0.5 μm, respectively.

3.2 External bunch quality control: compression

A scheme similar with the one in the preceeding section (see [21]) can be adopted to tackle the issue of bunch compression in plasmas when dealing with external injection. Compression schemes are at presently investigated because they might allow the matching conditions of LWFA to be matched at higher electron densities. In the scheme described in [21], the electron bunch is set to propagate initially in a low density plasma so that its length is much smaller than the plasma wavelength and its velocity smaller than the phase velocity of the wave. The bunch is injected close to the node of the plasma wave where the transverse forces are focusing. The gradient of the longitudinal force induces a longitudinal bunch compression, which forces particles to accumulate close to the trapping point. Figure 5 shows the results of a numerical simulation carried out using a 2D-cylindrical fluid code for the cold plasma in the quasi-static approximation. The code includes fully relativistic, nonlinear, space-charge and beam-loading effects and uses an optimised mesh size depending on the local pulse waist and plasma density. In the code, a 10 pC, 10 MeV electron bunch with a 60 μm full longitudinal size is injected in the node of the plasma wave generated by a 50 fs laser pulse in a plasma with a density of 5×10^{16} cm^{-3}.

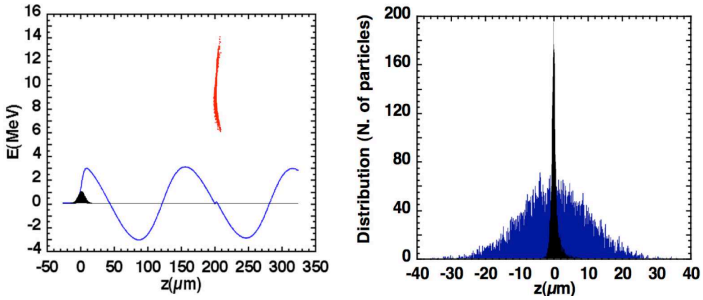

Figure 5: *Numerical simulation of bunch compression in an electron plasma wave. (left) The electron bunch after compression around the node of the longitudinal field of the electron plasma wave. (right) Comparison between the initial longitudinal bunch distribution and the same distribution after compression.*

The plots of Figure 5 clearly show the effectiveness of this bunch compression scheme. In particular, in the case presented an electron bunch with an initial 60 μm full size (10 μm rms) has been compressed by a factor of roughly 10 down to a 7 μm full size (1 μm rms). These parameters set the conditions for the second accelerating stage, whose modelling is at present in progress. Here we point out that with a bunch length after compression such as the one obtained in the simulations presented, the accelerating stage can take place even with a moderately high plasma density of the order of $1 - 5 \times 10^{17}$ cm^{-3}, which corresponds to an accelerating plasma wave wavelength shorter than 100 μm. This would allow the electrons to gain 1 GeV of energy on a spatial scale of 10 cm, while keeping the final energy spread down to a few percent, It is also worth to note that in order to accomplish to such a task one would need, in the case of a 50 μm waist size pulse, to guide the laser radiation over roughly 10 Rayleigh lengths, possibly with additional control of the phase velocity of the accelerating wave (via channel tapering). and represents a significant progress of the external injection scheme originally planned which required a plasma density well below 10^{17} cm^{-3}.

3.3 Thomson scattering source modelling

The PLASMON-X approach to Thomson scattering includes a configuration based upon the use of the LINAC-produced electron bunches, and a more advanced configuration based upon the use of electron bunches generated by LWFA. Ultrashort, intense laser pulses offer unique opportunities to activate novel regimes of X-ray generation processes [14]. TS from free electrons is a purely electro-dynamic process in which each particle radiates while interacting with an electromagnetic wave.

The first configuration has been investigated and modelled in several different operating modes, including the High-Flux-Moderate-Monochromaticity (HFM2) mode and the Short and Monochromatic (SM) operating mode. A detailed description of these two regimes, which can be found in [23], was obtained with the aid of a Monte Carlo code named Thomson Scattering Simulation Tools, $(TS)^2$ [24], which accounts for the actual focusing of the laser beam with the possibility of implementing propagation up to multiple Rayleigh length via pulse guiding. The code also includes full treatment for non-linear effects (multi-photon absorption), an accurate description of the electron bunch emittance effects and non-perfect pulse-bunch overlapping. In the second configuration, LWFA-generated electron bunches with controlled injection are used as an alternative to conventional LINAC-accelerated electron bunches. As already discussed above, injection by longitudinal nonlinear breaking of the wave at a density downramp is one of the most promising way of achieving e-beams having both low energy spread and low transverse emittance. Simulations of the LWFA process were performed with a fully self-consistent Particle-In-Cell (PIC) code in the 2.5D (3D in the fields, 2D in the coordinates) configuration. A full description of the numerical design of this configuration is reported in [23]. Here we summarise the final result obtained for the expected performances of the FLAME laser system.

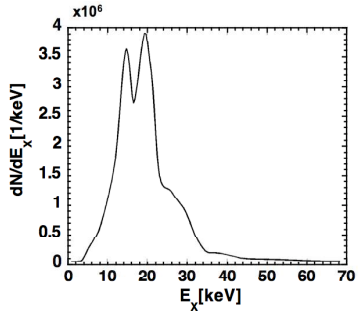

Figure 6: *Spectrum of the TS radiation of the ultra-short source in the case of a normalized acceptance angle of 0.5 deg.*

The numerical results therefore show that the head-on collision of the 20 pC e-bunch with a 5J, 5ps laser pulse focused with a 15μm waist might produce a 1 fs-long X-ray pulse with mean energy 20 keV at the fundamental frequency, an energy spread of 25% rms and with a total flux of 10^8 photons/shot (i.e. photons/s @10Hz). The duration of the scattered radiation is thus remarkably small (less than 1 fs). This result, still under further validation with a fully 3D configuration, therefore strongly suggests the possibility of achieving an ultra-short, hard X-ray source.

4 Conclusions

The PLASMON-X experiment will make use of complex hardware consisting of the most advanced LINAC technology and the most powerful. high repetition rate laser system ever built. The aim

is to demonstrate the possibility of achieving an high quality acceleration of externally injected bunches, together with the generation of tunable hard X-ray radiation. At the same time, the most recent progress in the control of laser driven acceleration opens the way to complementary, all-optical schemes for X-ray generation that offer the opportunity of unique performances in terms of ultra-short pulse duration. The construction of the required infrastructure, namely the FLAME laboratory is under construction. Parallel to this, theoretical and numerical modelling is being carried out to further validate experimental parameters and to study even more advanced schemes.

References

1. D. Alesini et al., Proceedings of EPAC 2006, Edinburgh, Scotland, p. 2439.
2. D. Alesini et al., NIM-A **507**, 345 (2003).
3. D. Strickland and G. Mourou, Opt. Comm. **56**, 219 (1985).
4. T. Katsouleas, Nature **431**, 515 (2004).
5. S.P.D. Mangles *et al.*, Nature **431**, 535 (2004).
6. C.G.R. Geddes *et al.*, Nature **431**, 538 (2004).
7. J. Faure *et al.*, Nature **431**, 541 (2004).
8. W. Leemans *et al.*, Nature Physics **2**, 696 (2006).
9. L.A. Gizzi *et al.*, Phys. Rev. E **74** 036403 (2006).
10. A. Giulietti *et al.*, Phys. Plasmas **13**, 093103 (2006).
11. A. Gamucci *et al.*, Appl. Phys. B **85**, 611 (2006) .
12. T. Hosokai *et al.*, Phys. Rev. E **73**, 036407 (2006) .
13. S. Kar *et al.*, New J. Phys. **9**, 402 (2007).
14. L.A. Gizzi *et al.*, Plasma Phys. Contr. Fus. **49**, B211 (2007).
15. R.H. Milburn, Phys. Rev. Lett. **10** 75 (1963).
16. C. Bemporad *et al.*, Phys. Rev. **138**, 1546 (1965).
17. W. P. Leemans *et al.*, Phys. Rev. Lett. **67** 1434 (1991).
18. P. Tomassini *et al.*, IPCF-CNR Internal Report (2002).
19. P. Tomassini *et al.*, Phys. Plasmas **10**, 917 (2003).
20. L. Labate *et al.*, Nucl. Instr. And Meth. A **495**, 148 (2002).
21. S. V. Bulanov *et al.*, Phys. Rev. E **58** 5, R5257.
22. P. Tomassini *et al.*, Phys. Rev. ST-AB **6** 121301 (2003).
23. P. Tomassini *et al.*, Proc. of the LPAW 2007, IEEE TRANS. ON PLASMA SCI. (2007), in press.
24. P. Tomassini *et al.*, Appl Phys B DOI:10.1007/S00340-005-1757-X (2005).
25. A. L. Cavalieri *et al.*, Phys. Rev. Lett. **94**, 114801 (2005).

From LNF-INFN report 2008

NTA PLASMONX

C. Benedetti, P. Londrillo, S. Rambaldi, G. Turchetti
Sezione INFN Bologna

R. Bonifacio, M. Castellano, A. Clozza, L. Cultrera, G. Di Pirro, A. Drago, M. Esposito, M. Ferrario, D. Filippetto, A. Gallo, G. Gatti, P. Gaudio, A. Ghigo, A. La Monaca, M. Migliorati, D. Nanni, L. Palumbo, M. Richetta, C. Sanelli, F. Tazzioli, A. Tenore, F. Terra, S. Tomassini, C. Vaccarezza, C. Vicario
Laboratori Nazionali di Frascati

A. L. Bacci, F. Broggi, M.M. Cola, A. Flacco, C. Maroli, M. Passoni, V. Petrillo, N. Piovella, R. Pozzoli, M. Romé, A. R. Rossi, L. Serafini
Sezione INFN Milano

D. Batani, A. Galassi, G. Lucchini, R. Jafer, R. Redaelli, R. Benocci, T. Desai
Sezione INFN Milano Bicocca

U. De Angelis, S. De Nicola, R. Fedele, G. Fiore, C. Stornaiolo
Sezione INFN Napoli

S. Betti, C.A. Cecchetti, A. Giulietti, D. Giulietti, A. Gamucci, L.A. Gizzi, P. Koester, L. Labate, T. Levato, A. Macchi, P. Tomassini, M. Vaselli
Sezione INFN and CNR Pisa

1 Summary

The 2008 has been a very fruitful year for the NTA-PLASMONX project. The laser laboratory has been completed and equipped, the laser FLAME assembled and tested at Amplitude Technologies laboratories, the first Laser-Plasma Acceleration experiment (full Italian!) successfully performed in Pisa, new experimental results useful for the project main goals obtained at European laser facilities and at BNL, the design of the e-beam and interaction chamber for the Thomson Scattering based X-ray source completed. Moreover the theoretical and simulation groups have fully supported the experimental activity and anticipated the future scenario of the LPA experiments and X-ray innovative sources that will be carried out in the very next future at LNF. All that will be shortly presented in the following.

2 FLAME

During 2008, construction of the FLAME laser system was carried out at Amplitude Technologies, following requirements and specifications defined during the tender procedure. Several visits of the FLAME team were carried out at Amplitude, including a session for measurements on timing and synchronization, a preliminary acceptance test and a final acceptance test. Final tests included full system energy measurements, survey of the pulse duration optimization procedure, pulse duration measurer nents, including the control-command interface (see Figure 1).

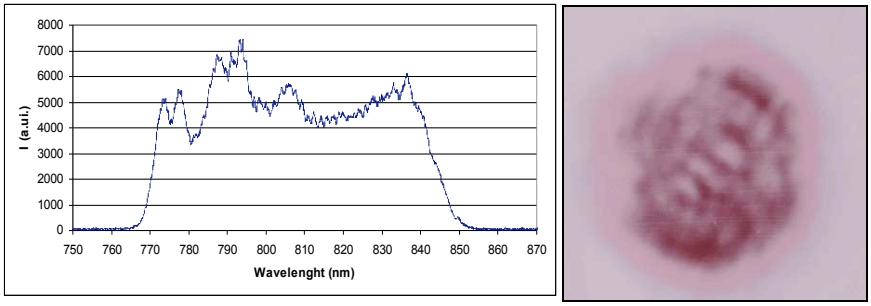

Figure 1: *Left: Spectrum of the laser pulse after amplification showing a bandwidth exceeding 70 nm. Right: Single shot 7 J burn pattern.*

The main parameters of the system measured during the final acceptance test at the factory, during full energy operation at 10 Hz rep. rate are: 5.6 J (energy after compression); 23 fs (pulse duration); 250 TW (peak power), $< 10^{10}$ (ASE contrast); $< 10^{-8}$ (pre-pulse contrast). The average energy (before compression) was measured to be 7.07 J.

3 FLAME laboratory

During 2008 the construction of the FLAME building was completed as shown in the Figure 2 and the design of the entire laboratory layout was carried out including all main subsystems and components: clean room for hosting the laser system, beam transport to the FLAME underground target area and to the SPARC bunker, electricity and ethernet networks, water cooling and air conditioning. Detailed design of the FLAME target area for the planned test experiment on self-injection was also carried out. Procurement for the construction of the beam transport vacuum line and for the set up of the test experiment was started, including the main mirrors, the focusing off-axis parabola and the main experimental diagnostics (see Figure 3).

Figure 2: *FLAME building at LNF completed on 23rd June 2008.*

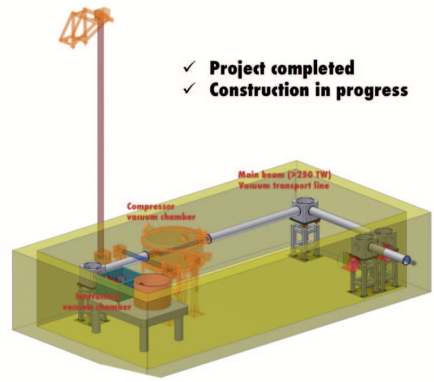

Figure 3: *Design of the layout of the underground target area of the FLAME laboratory, with the main compressor chamber, the vacuum transport line and the target chamber for laser-only experiments.*

4 Laser-Plasma Acceleration Experiment at ILIL-CNR/PISA: First Results from the Plasmon-X Project

4.1 The experimental set up

In the experiment, the main pulse was focused onto a gas-jet target using an F/6 off-axis parabola. The gas-jet target was irradiated at full laser energy varying the gas backing pressure, (i.e. the pressure in the pipe before the fast valve controlling the nozzle) to change the value of the maximum density of the neutral gas. Two gases were used in our experiment, namely He or N_2.

Characterisation of the neutral gas was carried out using optical interferometry. The use of two gases He and N_2, enabled us to explore targets characterised by dfferent physical properties mainly related to the atomic number, and, in particular, to the ionization properties under irradiation of ultrashort, intense laser pulses. The gas-jet nozzle was characterised by a 4 mm long, 1.2 mm wide slit and was mounted on a micrometric motorized support in order to move the interaction point along the three cartesian axes (position scan). During the pulsed operation, the gas flows out of the slit at supersonic speed in order to produce steep interfaces between gas and vacuum. The vacuum in the chamber before the shot is maintained at a pressure below $\approx 10^{-4}$ Torr by a turbo-molecular pump connected to the chamber by a gate-valve.

A full scan of the position of the focal plane along the laser propagation axis and with respect to the top of the nozzle was performed to find the best conditions for acceleration. An important feature consistently observed throughout the experiment is that electron acceleration in our experimental conditions was always found to occur when the focal plane (waist) was located in the proximity of the near edge of the nozzle, typically at ≈ 0.6 mm from the top of the nozzle. A full scan in pressure was also performed, showing that at higher pressure more stable, but less collimated electron bunches are produced. Several diagnostics were used to study the laser-target interaction and the accelerated electrons as shown schematically in Fig. 4. Thomson scattering and Nomarski interferometry were set up perpendicularly to the main laser pulse propagation axis to study and characterize ionisation and basic laser-plasma interaction issues. A second group of

diagnostics including scintillators coupled to photomultipliers, a phosphor screen (LANEX), an electron spectrometer based upon permanent magnets and dose sensitive, radiochromic film stacks (SHEEBA), enabled indirect and direct detection and characterization of the electron bunches accelerated during the laser-gas interaction.

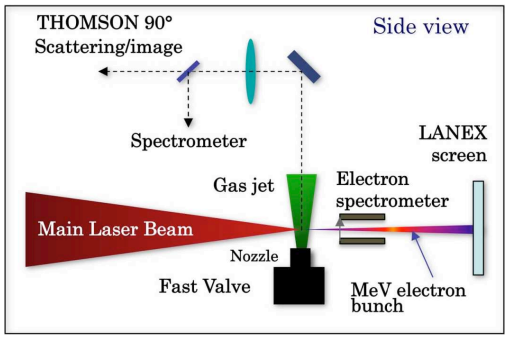

Figure 4: *Design of the layout of the underground target area of the FLAME laboratory, with the main compressor chamber, the vacuum transport line and the target chamber for laser-only experiments.*

4.2 Thomson scattering

Thomson scattering diagnostic was used throughout the experiment to monitor interaction conditions and to identify the basic plasma parameters (see Figure 5). In the classical picture of Thomson scattering, the electrons oscillate in the laser field and, in turn, emit radiation.

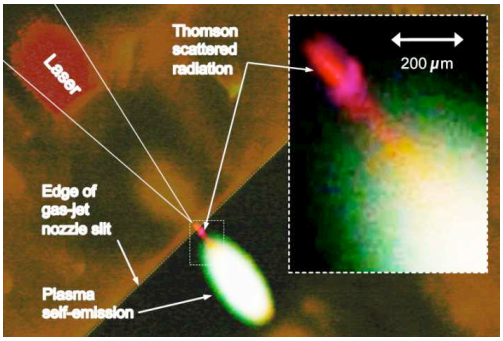

Figure 5: *Typical top-view image of the gas-jet nozzle obtained by the Thomson scattering diagnostic channel showing the main features of the interaction. The waist of the laser beam is placed on the edge of the gas-jet where Thomson scattering radiation is clearly visible (red in colour image). Beyond that point, the laser beam expands and the emission visible in the image is dominated by white light plasma self-emission. The insert in the top-right side of the image shows the magnified region of interaction.*

The properties of this scattered radiation are thus related to the properties of the medium and provide combined information on the laser intensity and electron density. Since in our case, knowledge on the plasma density can be derived independently from the plasma interferometry,

we can use Thomson scattering to derive information on the laser intensity. In our experimental set up an F/10 achromatic doublet was used to produce a 10X magnied image of the interaction region. The image of Fig. 5 shows an overview of the emission produced along the entire laser propagation axis. The waist of the laser beam is placed on the edge of the gas-jet (dashed line in the image) and Thomson scattering radiation is clearly visible as a $\approx 200\,\mu$m long channel-like structure.

A spectral analysis of the accelerated electrons was carried out using a magnetic spectrometer coupled with the LANEX screen (see Figure 6). The spectrometer, based upon permanent NeFeB magnets generating a quasi-uniform magnetic eld ($B_{Max} \approx 0.45$ T), was placed at a distance of 44 mm in front of the LANEX screen. The magnetic field amplitude was mapped in the region of interest using a millimeter-sized Hall magnetic probe. A 2 mm thick Pb foil with a 0.5 mm slit width was placed in front of the magnet, with the slit direction parallel to the magnetic field, in order to limit the transverse momentum of electrons accepted by the electron spectrometer and consequently to increase the resolution of the spectrometer (see Figure 7).

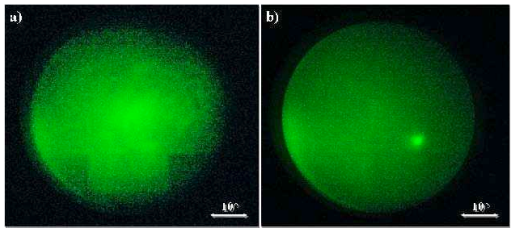

Figure 6: *Typical outputs of LANEX in detection conguration. a) non collimated laser-accelerated electrons in case of N_2 gas at 50 bar. b) collimated laser-accelerated electron bunch in case of He gas at 50 bar.*

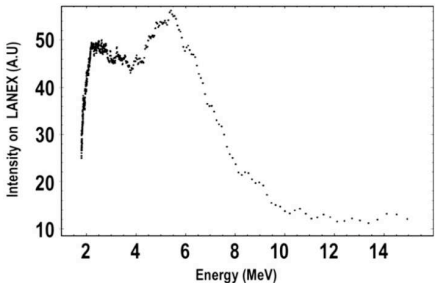

Figure 7: *Electron spectrum obtained with the magnetic spectrometer showing quasi monoenergetic peak between 5 and 6 MeV. The spectrum was obtained from irradiation of a N_2 gas-jet at a backing pressure of 45 bar.*

Numerical modeling based upon particle tracing in the mapped magnetic eld was implemented to describe the performance of the spectrometer in order to obtain the dispersion curve and the intrinsic resolution of both the imaging acquisition system and the LANEX screen. The code also account for errors introduced by beam pointing instability and space-charge effects along

propagation. The results obtained by the magnetic spectrometer were confirmed by independent measurements carried out using an energy spectrometer consisting of sandwiched Radiochromic films (RCF). A sample spectrum obtained with the magnetic spectrometer with N_2 gas-jet is displayed in Fig. 7. According to this spectrum, electrons up to 10 MeV were detected, with an overall spectral distribution characterized by a broad peak with a maximum between 5 and 6 MeV. In some shots, narrower spectral components were found, thought with a poor reproducibility. These results confirm that, in spite of the very low laser intensity compared with most of the experiments available in literature, the electrons accelerated in our experimental conditions are well in the multi-MeV region, with evidence of mono-energetic components emerging clearly from the broad energy spectrum.

4.3 Efficient electron acceleration with 10 TW laser pulses and possible medical applications

In order to improve the characteristics of an electron bunch coming from ultra-intense laser-plasma interaction, an experiment was performed at the SLIC laboratory of CEA Centre in Saclay (France) with a 10 TW Ti:Sa laser system delivering pulses with duration of 65 fs (FWHM) at a wavelength of 800 nm, accounting for a laser strength parameter $a_0 \leq 2$. The experiment, carried out jointly by the ILIL group of CNR, Pisa with the host PHI (Physique a Haute Intensite) group, plus a group from LULI (Ecole Polytechnique, France) and a group from ITU (Institute for Transuranium Elements, Karlsruhe, Germany), allowed the best interaction conditions between the laser pulse and a supersonic gaseous target to be found, and stable and reproducible electron bunches with energy in the range 10-45 MeV to be accelerated (Fig. 8). This task is very important in the context of the comprehension of the mechanisms involved in the laser-plasma interaction and acceleration process (with particular attention to the propagation process) in order to produce high-energy electron bunches. Improvements in the comprehension of such phenomena will be in turn exploited in the frame of the project PLASMONX at ILIL and the Laser Facility that will be soon operating at LNF.

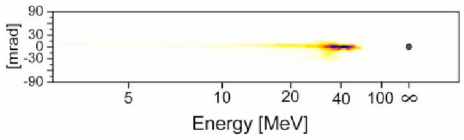

Figure 8: *Representative calibrated image from the magnetic spectrometer. Accelerated electrons show a mono-kinetic component with energy as high as 40 MeV.*

Several advanced diagnostics have been employed to monitor the interaction and the accelerated electron bunches. The photo-activation of nuclear material $^{1}97Au$ driven by the high-energy electrons bremsstrahlung (Fig. 9) in a suitable converter has also been employed to get the number of particles in the bunch with a high degree of accuracy. The total number of electrons with energy greater than 3 MeV was found to be (3.15 ± 0.13) x 10^{10} per laser shot, evinced consistently from all the employed diagnostics. The presented efficient electron source contributes to indicate laser driven electron accelerators, provided them stability and reliability, as a suitable source for medical uses, in particular for Intra-Operative Radiation Therapy (IORT) of tumors. The main properties

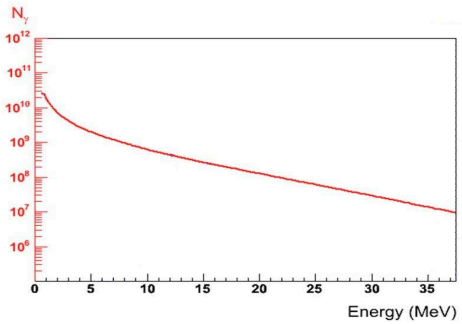

Figure 9: *Spectrum of the bremsstrahlung gamma yield obtained after interaction of the accelerated electrons in a tantalum converter. The number of electrons found after comparison with Monte Carlo tracking code is (3.15 ± 0.13)* $\times 10^{10}$ *per laser shot.*

of commercial RF Hospital accelerated electron bunches for IORT treatment and those of this laser driven accelerator are comparable in terms of bunch charge and electron energy. However, although the dose delivered for each shot is also comparable, the electron bunch duration is about six orders of magnitude lower in the case of the laser-plasma accelerator: few picoseconds versus few microseconds. Thus, the peak current is approximately a million times higher. The radiobiological effects of such difference are still unknown. The new ultrashort laser-plasma electron source thus opens an exciting field of basic bio-medical research.

4.4 Theory and simulations for self-injection experiments

We present some theoretical/numerical studies on electron acceleration (self-injection configuration) with the parameters of the FLAME laser, considering half of the maximum nominal power (P = 150 TW instead of 300 TW), in view of the first LPA experiments which will be carried out during 2009 for the commissioning of the laser system. In order to check the predictions of the scaling laws we have performed several 2D/3D simulations for the 1.2 mm gas-jet. Two-dimensional simulations to study the production of GeV electrons (propagation lengths of $\approx$ 6 mm are required) are underway. All the simulations have been carried out with the fully self-consistent, relativistic, parallelized PIC code ALaDyn. We acknowledge the support of the CINECA computing center for the 3D runs (grant: Simulazioni PIC 3D per l'accelerazione laser-plasma).

- Case 1: We consider $w_0 = 8.9$ μm ($I \approx 1.2 \times 10^{20}$ W/cm^2) and $n_e = 10^{19}$ cm^{-3} (Lgas-jet = 1.2 mm). In Figure 10 (left, center) we show the electron density (XY cut) and the electron energy spectrum. Already inside the plasma (0.7 mm from the beginning of the gas-jet) we observe a monochromatic peak E = (160 ± 5) MeV (FWHM) with a charge of 0.45 nC. Unfortunately we observe also a significant erosion of the laser-pulse front (causing an anticipate dephasing not predicted from the scaling laws) which limits the energy gain for the electrons (160 instead of 400 MeV). This phenomenon has been observed in several 2D simulations when the plasma density is higher than 10^{19} cm^{-3} and the laser is intense. In Figure 10 (right plot) we plot the transverse (x -px) phase space for the monochromatic bunch. The r.m.s. amplitudes of the bunch are $\approx$ 0.8 μm (transverse) and $\approx$ 2.5 μm

(longitudinal), while the normalized emittances are ≈ 5 mm mrad. The (high) value of the emittance is related to the large transverse momentum of the trapped particles and seems to be an unavoidable feature of the bubble regime, however, working at lower laser intensities can give some advantage in this respect.

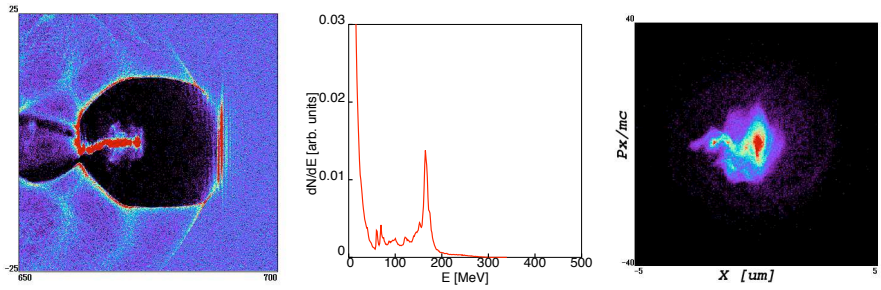

Figure 10: *Case 1:* $w_0 = 8.9\ \mu m$ *(*$I \approx 1.2\ 10^{20}\ W/cm^2$*) and* $n_e = 10^{19}\ cm^{-3}$ *(Lgas-jet = 1.2 mm). (left, center) the electron density (XY cut) and the electron energy spectrum. (right plot) the transverse (x-px) phase space for the monochromatic bunch.*

- Case 2: We consider $w_0 \approx 12\ \mu$m (I $\approx 6 \times 10^{19}$ W/cm^2) and $n_e = 6 \times 10^{18}$ cm^{-3} (Lgas-jet = 1.2 mm). The predicted maximum energy is ≈ 440 MeV and the dephasing length is longer than the gas-jet length so we dont expect a monochromatic beam at the end of the simulation. In Figure 11 we plot the electron spectrum at the exit of the gas-jet and we find a broad peak with an energy of E = (420 ± 40) MeV (FWHM), the corresponding charge is 0.4 nC. Both values are in agreement with theory. The r.m.s. amplitudes of the bunch are ≈ 0.5 μm (transverse) and ≈ 1 μm (longitudinal), the normalized emittances are ≈ 2.5 mm mrad.

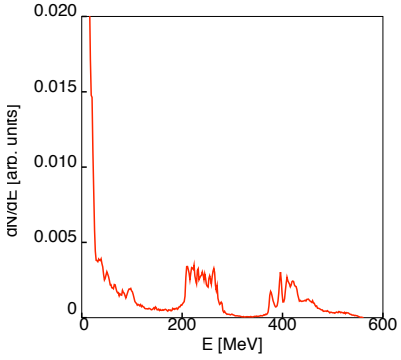

Figure 11: *Case 2:* $w_0 \approx 12\ \mu m\ I \approx 6 \times 10^{19}\ W/cm^2$*)* $n_e = 6 \times 10^{18}\ cm^{-3}$ *(Lgas-jet = 1.2 mm).*

4.5 External Injection: a route for multi GeV high-quality e-beams

4.5.1 Goals and acceleration scheme

The aim for the external-injection studies were the search of an innovative scheme for the generation of multi-GeV beams with promisingly good slice quality and acceptable projected emittances. High-gradient acceleration requires relatively high plasma densities (10^{17}-10^{18}) cm^{-3} that are linked to electron plasma waves in the range (30-100) μm. Since beam-quality requirements are tight, injected beam length is one of the crucial parameters of the scheme and for a 100 μm long wave beam monocromaticity requires injected bunches having lengths not exceeding 2-3 μm rms, a challenging result for current RF-photoinjector technology. Other critical issues are emittance preservation that has been achieved by using an adiabatic injection scheme (i.e. injection in the wake of an adiabatically focusing laser pulse), acceleration length elongation (that should be extended up to 20 Reyleigh lengths via pulse guiding), detailed Langmuir wave phase control that has been obtained via appropriate plasma profile tailoring and jitter of the injection phase. Another issues are nonlinear dynamics of the laser pulse that may undergo self-focusing or phase-modulation and pulse erosion.

4.5.2 Simulation tools

Simulations were performed with the **QFluid** code [P. Tomassini, 2005-2008] that solves in the quasistatic approximation nonlinear equations of fluid response to ponderomotive forces of the laser pulse and beam-loading effects. The **QFluid** code works in a 2D cylindrical space and it has been tested with ALaDyn. The code does not take into account for laser pulse nonlinear dynamics and erosion. While pulse erosion in 10cm should be negligible since the pulse strength a_0 reduces by less the 4% [1D PIC results], detailed self-consistent simulations should be performed for studying pulse nonlinearities.

4.6 Simulation results

A 25 pC, 5 μm and 2.5 μm of rms transverse and longitudinal sizes, energy of 150 MeV and transverse normalized emittance of 1 mm·mrad electron bunch is injected in the second bucket of the Langmuir wave excited by a Ti:Sa pulse delivering 7 J of energy in 30 fs. The laser pulse with initial waist size of 130 μm and minimum size of 32.5 μm is guided by a matched channel profile. The plasma is 9.88 cm long and its density profile has a positive and varying slope with starting and ending densities of 1.5×10^{17} cm^{-3} and 2.5×10^{17} cm^{-3}, respectively. At the final simulation step (see Figure 12) a 2.2GeV electron beam with global energy spread and emittance of 4% rms and 1.5 mm·mrad, respectively, is produced.

Slice analysis with slice thickness of 250 nm reveals the potentialities of the bunch as a driver in X-FEL. While slice emittance is in the range (1.2-1.4) mm.mrad the slice energy spread is in the range (0.02-0.1)% for slices 8-13, with a local current of about 1kA.

5 Ion Laser-Plasma Acceleration

Ion acceleration from solid targets irradiated by high-intensity pulses is a burgeoning area of research, currently attracting a phenomenal amount of experimental and theoretical attention

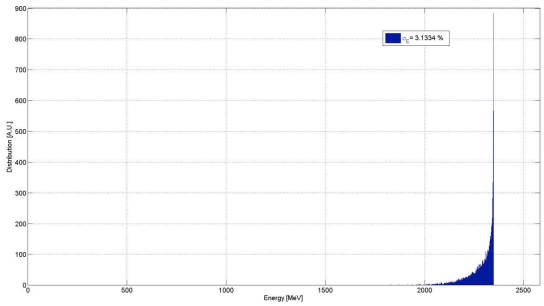

Figure 12: *Energy distribution of the produced e-bunch.*

worldwide. Key to this interest are the ultra-compact spatial scale of the accelerator and the fact that the properties of laser-driven ion beams are, under several respects, markedly different from those of "conventional" accelerator beams. In particular, the spatial quality of laser-driven beams is exceptionally high, and their duration at the source is - down in the ps scale - orders of magnitude shorter than other available sources. In view of such properties laser-driven ion beams have the potential to be employed in a number of innovative applications in the scientific, technological and medical areas, where proton beams with energies greater than 100 MeV are of interest. The FLAME laser could be ideally suited to perform experimental campaigns aimed at improving our basic understanding in this area, towards the achievement of "true" ion beams for applications. In this context, within the PLASMONX project a working group devoted to this subject has been established. A research program has been identified, with the following specific goals:

1. Study and development of dedicated beam diagnostic in order to characterize the quality, the control and the reproducibility of the ion beams, with methods and techniques which are typical of the accelerators physics and technology.

2. Theoretical and experimental investigation of the acceleration mechanisms of ions in the interaction of the ultrashort superintense FLAME laser pulses with solid targets, aimed at the improvement and optimization of the beam properties.

5.1 Theoretical and experimental activity on the TS-source

i) The design of the laser-beam interaction chamber and the devoted e-beam:

A complete design of the interaction chamber, with the focussing solenoid, the bending dipole for the dumping of the beam, the screening of the interaction region and the laser path is presented in Fig. 13. The technical design of the e-beams devoted to the TS based source and the LPA of the external injected electrons has been completed (see Fig. 14).

ii) The development of a procedure of optimization of the X-rays photon flux by means of a genetic algorithm:

In the framework of the maximization of the photon flux of the X radiation produced by the TS source, the genetic code ALGEN has been developed with the aim of optimizing the beam line. The beam line used is similar to that adopted in previous simulations for the

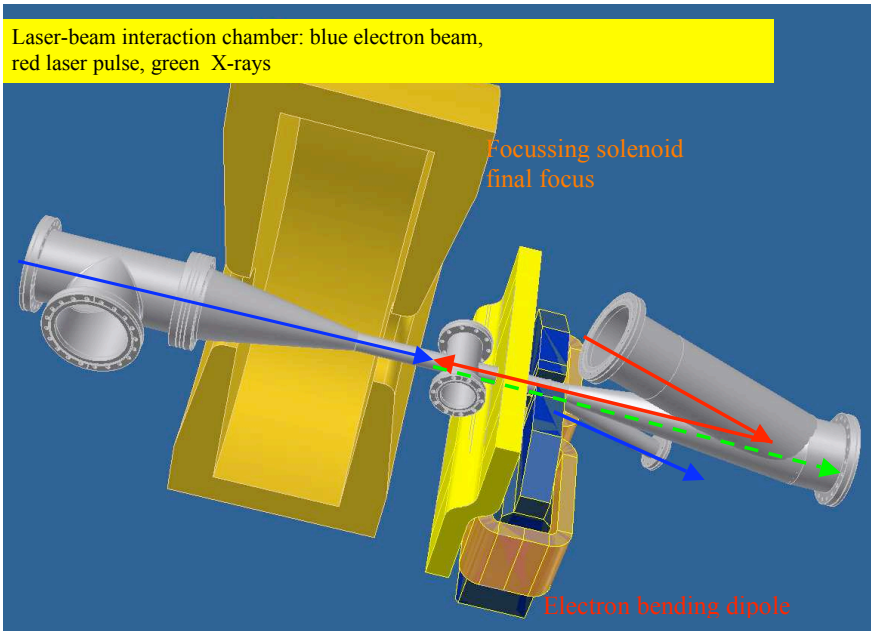

Figure 13: *Interaction chamber for Thomson Scattering based source.*

SPARC/PLASMONX experiment. The bunch has total charge of 1 nC and is extracted from the cathode with a laser pulse of 30 ps. The optimization plays with the following parameters: the gradient of the electric field of the gun $\mathrm{d}E_g/\mathrm{d}z$, the injection phase in the gun Φ_g, the maximum magnetic field of the gun B_g, the gradients of the accelerating structures $\mathrm{d}E_n/\mathrm{d}z$, the injection phase in the structures Φ_n, the maximum magnetic fields B_n, the position of the solenoids zn, and injection phase and position of the forth harmonic cavity Φ_{IVH} and z_{IVH}.

iii) The temporal structure of the X-ray electric field, the field phase and the impact that these characteristics can have on the phase contrast imaging have been considered. For the application to the phase contrast imaging it is very important to determinate the degree of spatial coherence of the radiation. In fact, the electrons of the beam have initial positions and velocities randomly distributed. The inherent randomness of the source will reflect itself on all parameters and measured quantities of the process.

iv) The participation to the measurements of imaging at the TS-source at ATF (BNL, Brookhaven) and the application of these tools to them:

Cooperation with the BNL group working at ATF has been initiated, with the participation of members of the PlasmonX experiment to the measurements made along 2008 on the TS source of Brookhaven. The measurements regard the use of the phase contrast technique for the imaging of wires of various materials and dimensions. A measure of the X rays spot with the traces of the wires has been performed. The X-intensities as given by a phase contrast simulation for a pet wire of dimension of 200 micron have been afterwards evaluated.

v) The investigation of other possible X radiation schemes (All Optical Thomson Source, AOFEL):

Other possible X radiation schemes (All Optical Thomson Source, AOFEL) have been invesigated. In particular we have studied the generation of low emittance high current monoenergetic beams from plasma waves driven by ultra-short laser pulses, in view of achieving beam brightness of interest for FEL applications. The aim is to show the feasibility of generating nC charged beams carrying peak currents much higher than those attainable with photoinjectors, together with comparable emittances and energy spread, compatibly with typical FEL requirements. We have focused on the regime based on a LWFA plasma driving scheme on a gas jet modulated in areas of different densities with sharp density gradients, because it seems more promising in terms of beam emittance. Simulations carried out using VORPAL show, in fact, that in the first regime, using a properly density modulated gas jet, it is possible to generate beams at energies of about 30 MeV with peak currents of 20 kA, slice transverse emittances as low as 0.3 mm.mrad and energy spread around 0.4 %. This beams break the barrier of 1018 A/(mm·mrad)^2 in brightness, a value definitely above the ultimate performances of photo-injectors, therefore opening a new range of opportunities for FEL applications.

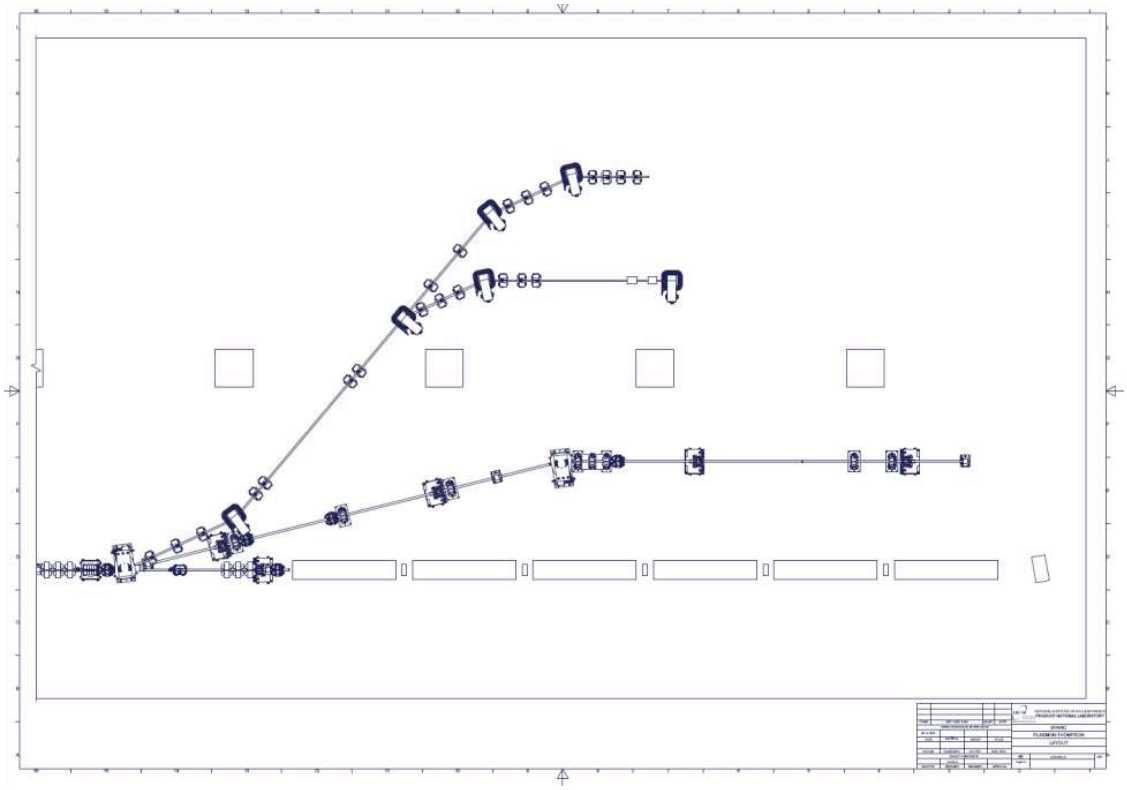

Figure 14: *The technical design of the e-beams devoted to the TS based source and the LPA of the external injected electrons.*

6 References

1. A. Giulietti *et al.*, Phys. Rev. Lett. **101**, 105002 (2008).
2. C. Benedetti, A. Sgattoni, G. Turchetti, and P. Londrillo, IEEE Trans. on Plasma Science, **36**, 1790 (2008).
3. L. A. Gizzi *et al.*, "An integrated approach to ultraintense laser sciences: the plasmon-x project", Europ. Phys. Journal - Special Topics 2009, in press.
4. A. Gamucci *et al.*, IEEE Trans. Plasma Sci. **36**, 1699 (2008).
5. C. Benedetti *et al.*, IEEE Trans. Plasma Sci. **36**, 1790 (2008).
6. C. Benedetti, A. Sgattoni, and P. Tomassini, "ALaDyn: a high accuracy code for the laser-plasma interaction", Proc. of EPAC08, Genova, Italy (2008).
7. C. Benedetti *et al.*, "PIC simulations of the production of high-quality electron beams via laser-plasma interaction", accepted for publication on Nucl. Instr. & Meth. A.
8. A. Bacci, C. Maroli, V. Petrillo, A. Rossi, and L.Serafini, Nucl. Instr. & Meth. in Phys. Res. B **263**, 488 (2007).
9. A. Cedola, I. Bukreeva, S. Lagomarisino, C. Maroli, and V. Petrillo, "Theoretical consideration for X-rays phase contrast mammography by Thomson Source", to be published on Nucl. Instr. & Meth. in Phys. Res. A.
10. P. Tomassini *et al.*, IEEE Trans. on Plasma Science **36**, 1782 (2007).
11. V. Petrillo, L. Serafini, and P. Tomassini, Phys. Rev. Spec. Top. Accel. Beams **11**, 070703 (2008).

From LNF-INFN report 2009

NTA PLASMONX

S. Bellucci, S. Bini, M. Castellano, A. Clozza, L. Cultrera, G. Di Pirro, A. Drago, M. Esposito, M. Ferrario, D. Filippetto, A. Gallo, G. Gatti, P. Gaudio, A. Ghigo, G. Giannini, A. La Monaca, T. Levato, F. Micciulla, M. Migliorati, D. Nanni, E. Pace, L. Palumbo, A. Petrucci, M. Richetta, C. Sanelli, A. Tenore, F. Terra, S. Tomassini, C. Vaccarezza, C. Vicario
Laboratori Nazionali di Frascati

C. Benedetti, G. Turchetti
Sezione INFN Bologna

A. L. Bacci, F. Broggi, M.M. Cola, A. Flacco, C. Maroli, M. Passoni, V. Petrillo, N. Piovella, R. Pozzoli, M. Romé, A. R. Rossi, L. Serafini
Sezione INFN Milano

D. Batani, R. Benocci
Sezione INFN Milano Bicocca

C.A.Cecchetti, A.Gamucci, D.Giulietti, L.A.Gizzi,
L.Labate, N.Pathak, F. Piastra
Intense Laser Irradiation Laboratory, INO-CNR and Sezione INFN, Pisa

N. Drenska, R. Faccini, P. Valente
Dip. Fisica Univ. La Sapienza, Roma

1 Introduction

In the 2009 the NTA-PLASMONX project [1] has seen the completion of the FLAME-laboratory and the installation start of the laser system previously tested at the Amplitude Technologies Laboratories. The main subsystem have been installed: the clean room, the laser, the cooling and the conditioning systems.
A self-injection test experiment (SITE) has been planned to establish the performance of the FLAME laser system and to assess the degree of control of critical laser parameters. The experimental setup has been realized and the study of a suitable MultiGev spectrometer has been performed to provide a device able to characterize the momentum of the GeV-class self-injected electrons of the SITE experiment. First measurement on a prototype have been carried on at the BTF facility at LNF.
The Interaction Region layout has been completed for the Thomson source experiment driving the procurement of the magnetic elements for the electron beam focusing system and of the multi-way vacuum chamber for the interaction point. The magnetic elements and the power supplies for the electron beam transfer lines have been committed together with the main components of the radiation transportation in vacuum. The description of this activity is given in the following.

2 FLAME

The FLAME laser (Amplitude Tech.) is based upon a Ti:Sa, chirped pulse amplification (CPA) system that will deliver 20 fs, 800 nm, up to 300TW, laser pulses with a 10Hz repetition rate at a fundamental wavelength of 800 nm. The system features a high, sub-ns contrast ratio ($> 10^{10}$) and has a fully remotely controlled operation mode. In the experiment, the main laser pulse is focused onto a gas-jet target using an F/10 off-axis parabola at a maximum intensity above $5 \times 10^{19} W/cm^2$.

Several optical and high-energy diagnostics including Thomson scattering, optical interferometry , scintillators coupled to photomultipliers, a phosphor screen (LANEX) and custom dose sensitive, radiochromic film stacks are under implementation to investigate laser-target interaction and the accelerated electrons. The 2009 has seen mostly the progress of the laser system installation and the fundamental steps can be summarized as follows:

- Jan-Mar: Laser system delivery at LNF completed
- May: Clean Room installation started
- Jun: "Cold" FLAME installation started: components in place
- Aug: Clean room fully operational
- Sep: FLAME laser start up: oscillator start-up and YAGs connections
- Oct: Compression test below 100 mJ level, YAGs pre-alignment and training
- Nov: Main amplifier pumps alignment, cryo amplifier installation (see figure 1)
- Dec: Main compressor optics aligned (see figure 2)

Figure 1: Main amplifier pumps alignment, cryo amplifier installation.

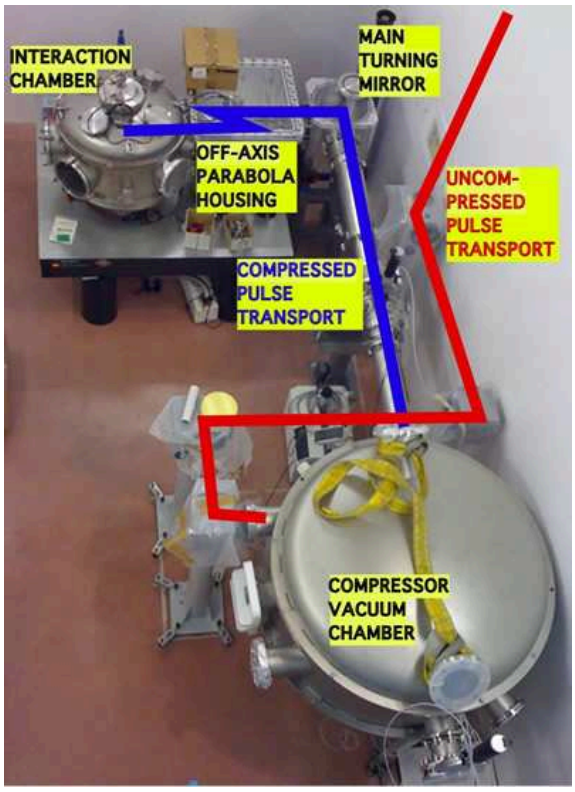

Figure 2: The SITE experiment setup with the main compressor optics aligned.

3 The SITE experiment

The self-injection test experiment at FLAME [2] aims at generating GeV-class electron bunches from laser-plasma interaction using a gas-jet of a few millimeters, working in the so-called bubble regime [3–5]. In the bubble regime a short ($c\tau < \lambda_p/2$) and intense ($a_0 > 2$) laser pulse expels the plasma electrons outward creating a bare ion column. The blown-out electrons form a narrow sheath outside the ion channel and the space charge generated by the charge separation pulls the electrons back creating a bubble-like wake. For sufficiently high laser intensities ($a_0 > 4$) electrons at the back of the bubble can be injected in the cavity and where the longitudinal accelerating field is of the order of $100\sqrt{n(cm^3)}V/m$ [7] . The FLAME laser meets both the two conditions of short pulse length and high intensity. As a consequence when the laser pulse impinges onto the gas-jet it promptly excites (without significant pulse evolution) a bubble wake where electrons are readily injected and so the entire gas-jet length can be utilized for the acceleration process. In order to have a controlled acceleration mechanism, which ensures a better final bunch quality, the plasma and laser parameters must be chosen according to the phenomenological theory described in [6]. A possible working point for the SITE is described in table 1.

In this case, following [6], a quasi-monochromatic (few % momentum spread) bunch is expected with a charge of 0.6 nC and an energy of approximately 1.0 GeV after 4mm (dephasing length). The acceleration process has been investigated also through 3D PIC simulations performed

Table 1: A possible working point of the test experiment on laser-acceleration at FLAME.

$L\_gasjet(mm)$	$n_p(e/cm^3)$	$\tau(fs)$	$I_0(W/cm^2)$	$w_0(\mu m)$
4	3×10^{18}	30	5.2×10^{19}	16

with the fully self-consistent, relativistic, electromagnetic PIC code ALaDyn [8, 9]. At the end of the simulation we obtained a bunch with an energy of 0.9 GeV and a momentum spread (rms) of 3.3 %, the charge is 0.6 nC, the bunch length is 1.8μm (the average current is 50 kA) and the beam divergence (rms) is 2.8 mrad. In Fig. 3 the resulting electron density at the end of the simulation is shown together with the. corresponding energy spectrum that shows two components, a peak with total charge $\approx 700pC$ at high energy (around 900 MeV) and a $\approx 3nC$ low energy tail.

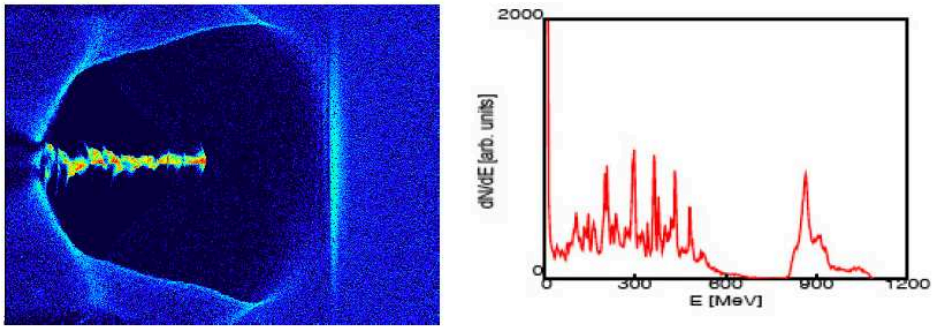

Figure 3: Results of the 3D PIC simulation: (left) electron density distribution shortly before the end of the acceleration and (right) out coming energy spectrum.

4 The Multi-GeV Electron Spectrometer

As shown in these simulations, experiments at FLAME will enter the GeV regime with almost 1nC of electrons. A spectrometer is being constructed to perform these measurements and it is made of an electro-magnet and a screen made of scintillating fibers for the measurement of the trajectories of the particles. From the high-energy point of view, this detector represents a challenge because it must measure the momentum spectrum of tens of millions of particles arriving simultaneously spread over three order of magnitudes in momentum (10 MeV to 10 GeV), and with a large (2mrad) divergence. Since the goal of the experiment is to find the optimal configuration to reduce the low energy tail and shrink the distribution of the high energy portion of the spectrum, the whole spectrum needs to be retained for all bunches. It is therefore not foreseen any form of focusing before the spectrometer (e.g. quadrupoles) since this would select only portions of the momentum spectrum. The transport of the electron bunches from the exit of the plasma to the spectrometer has been simulated with a 3D parallel tracking code for the beam dynamics of charged particles [10] in order to test possible collective effects in such high charge bunches. The position of the electrons when impacting on the optimized detector of the spectrometer as described later is shown in Fig.

4 with and without considering the electromagnetic interactions among the electrons. The effect is negligible, the resolution being dominated by the angular divergence of the beam at origin.

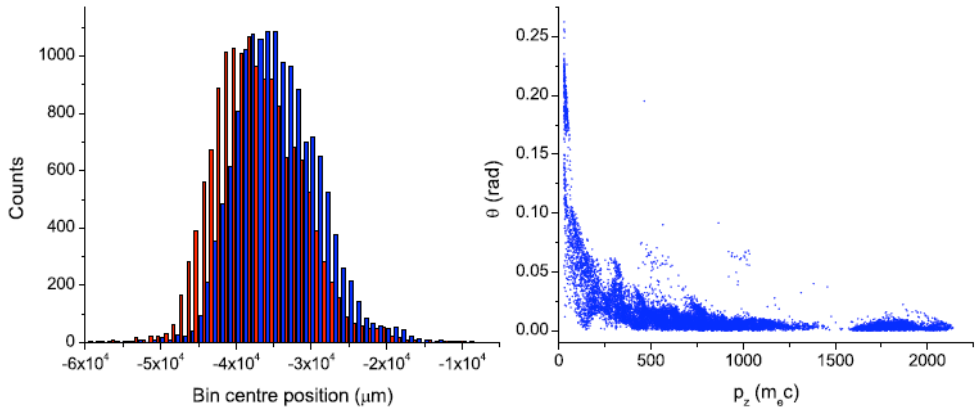

Figure 4: Left: generated (red) and reconstructed (black) momentum distributions overlayed. Right: resolution on momentum (blue squares) and the contribution from the position measurement only (red dots). The difference between the two is an estimate of the angular divergence.

For the purpose of designing the spectrometer, which is insensitive to the vertical position of the particles and to their direction of flight when impacting the detector, it is therefore sufficient to consider the motion of the particles on the horizontal plane (i.e. the one perpendicular to the magnetic field). This justifies why in the following the bunch is treated as a beam of independent particles coming from a point-like source located at the end of the gas-jet and with an angular divergence estimated with the simulation. Fig. 4 shows that the high energy particles are contained within 2 mrad, while the low energy tail can have a significantly larger divergence. To shorten the spectrometer set up schedule a spare magnet from the SPARC experiment will be employed, therefore the results shown below refer to an available but non-optimal magnetic setup. In Fig. 5 the experimental set-up is shown where the position detectors are located in such a way to intercept the low energy electrons (up to 150 MeV) at the focii of their trajectories and to collect as far as possible the higher energy ones in order to maximize the resolution of the energy measurement with the dispersive element.

A scintillating fiber detector has been chosen that could operate in vacuum, tolerate a large number of impacting particles and be of limited cost. The scintillating fibers Ku- raray SCSF-81-SJ with diameter $1.00 \pm 0.05mm$ have $50 \pm \mu m$ thickness of cladding and emission wavelength 437 nm. Fibers are connected to fvie multi- channel photo-tubes Hamamatsu H7545 (R7600-00) for a total of five PMT and 320 electronic channels. In order to read a larger number of fibers, since the overall resolution is not affected, the fibers coming from the low momentum detector are merged in groups of three. The choice of the front end card was studied in collaboration with INFN BA, GE and ISS-Roma1 [11].

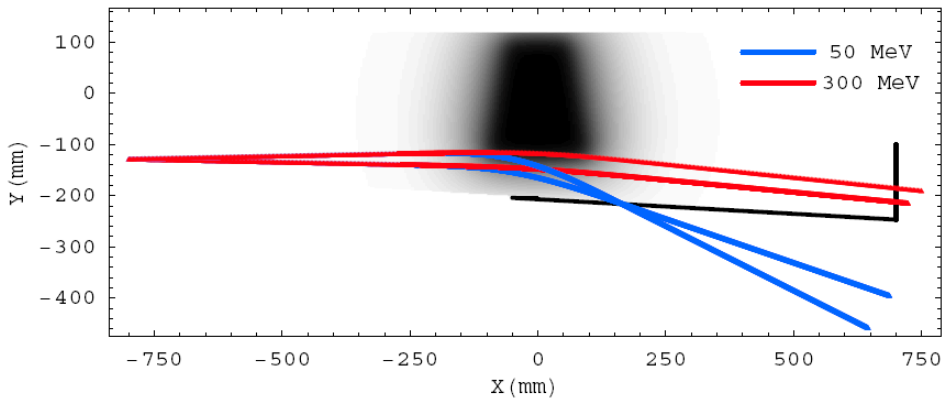

Figure 5: Trajectories in the available magnetic setup of particles with fixed momenta and divergence angle = ± 2 mrad. The position detectors are located along the black lines.

4.1 Estimated detector performance

Fig. 6 shows the effect of resolution from a fast simulation of almost mono- energetic beams. The worsening of the reconstruction with increasing momentum is clear. We also estimate the resolution of the detector, separating the intrinsic detector resolution caused by the physical dimension of the fibers (1mm of diameter) and the angular divergence. Fig. 6 shows the total resolution as a function of the momentum and the component due to the detector granularity. Performances between low and high detector will be different mainly because of the angular effect for the high energies. The pointing instability of the laser was also studied and our results show that the situation shown above is not significantly different even if these effects are of the order of degree. We can conclude that with the Prototype it is possible to measure energies up to 200 MeV with a very good resolution less then 1% and the resolution remains less then 5% up to about 500 Mev.

4.2 Tests with a prototype

A prototype with 64 fibers read by one PMT has been built and tested with electrons at the Frascati Beam Test Facility (BTF [12]) and in laboratory with LEDs. At the BTF test the electron beams was passing through the magnet that will be part of the detector, so that we could test the existence of the focii and the understanding of the fringe field region. The fact that the trajectories lie in the fringe area is in fact one the major concerns for this device. Fig. 7 shows that moving the beam from the center of the magnet to the fringe, the resolution, due to multiple scattering in air, improves and that the deviation of the beam as a function of the beam position is well reproduced by the numerical calculation.

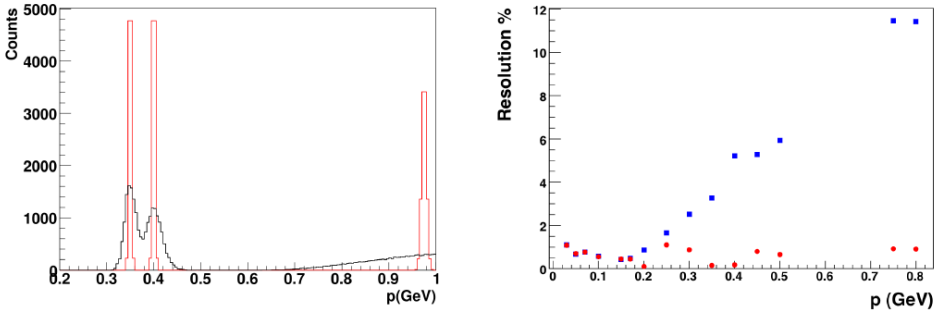

Figure 6: Left: generated (red) and reconstructed (black) momentum distributions overlayed. Right: resolution on momentum (blue squares) and the contribution from the position measurement only (red dots). The difference between the two is an estimate of the angular divergence.

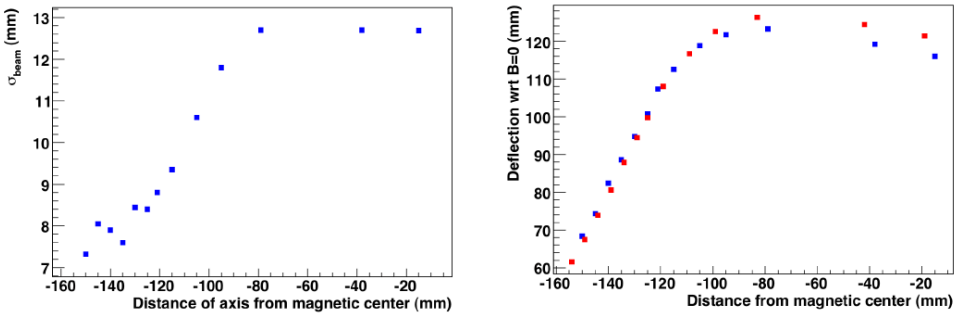

Figure 7: BTF test beam: (left) measured resolution as a function of the distance from the magnetic center and (right) comparison between prediction (red) and measurement (blue) for the beam deflection as a function of the position of the beam wrt the magnetic center.

5 The Thomson Source

Several experiments are foreseen within this facility, among the others: high gradient plasma acceleration as much as the production of monochromatic ultra-fast X-ray pulses by Thomson back-scattering(TS), which is hereafter pointed out [13]. TS X-ray source is attracting strong attention because of its flexibility and potential compactness with respect to conventional synchrotron sources. A TS source driven by high-quality electron beams can work in different operating modes, e.g.: the high-flux- moderate-monochromaticity-mode(HFM2) suitable for medical imaging when high-flux sources are needed; the moderate-flux- monochromatic-mode(MFM) suitable to improve the detection/ dose performance [14]; short-and-monochromatic-mode(SM) useful for pump-and-probe experiments e.g. in physical-chemistry when tens of femtosecond long monochromatic pulses are needed.

Table 2: Electron beam parameters at the interaction point.

Parameter	value
Bunch charge(nC)	$1 \div 2$
Energy (MeV)	$28 \div 150$
Length (ps)	$15 \div 20$
$\epsilon_{nx,y}$ (mm-mrad)	$1 \div 5$
Energy spread(%)	$0.05^{1} \div 0.2$
Spot size at interaction point rms (mm)	$5 \div 10$

Table 3: X-ray beam characteristics (numerically computed).

Parameter	Value
Photon energy (KeV)	$20 \div 500$
Photon per pulse (at 1nC for 6 mrad collected angle)	$1.5 \div 2.0 \times 10^{9}$

5.1 Electron beam and Thomson Interaction region

The electron beamlines design has been completed, with the capability to transport electron beams with energies ranging from 28 MeV up to150 MeV. The key point in electron beam transport is preserving the high brightness coming from the linac, hence ensuring a very tight focusing for the whole energy span.The final features that the electron beam will show at the interaction point, are reported in Table 2, while a nover all view of the PLASMONX beam lines within the SPARC hall is showed in Fig. 8.

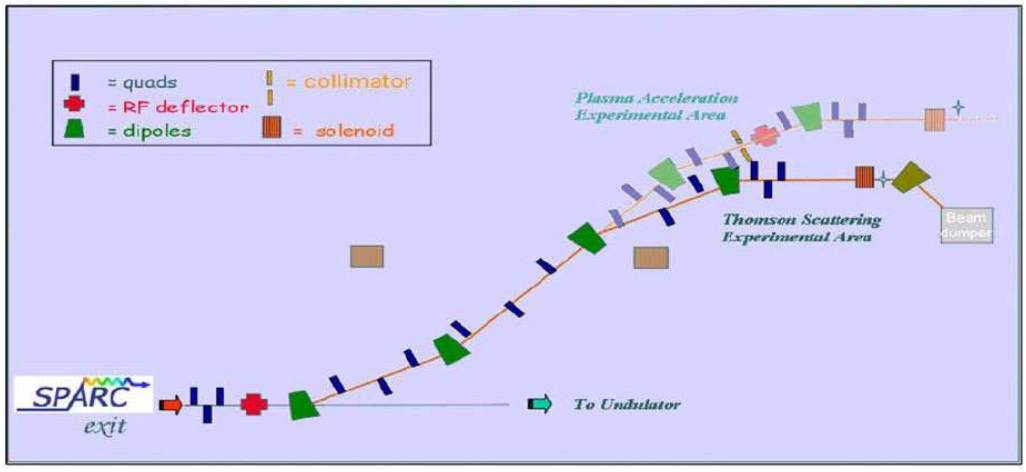

Figure 8: Lay-out of the dog-leg like electron beamline for the TS experimental area.

These properties of the electron beam are strictly necessary in order to reach the high X-ray beam flux as reported in Table 3 (10^9 photons/s with a rep.rate of 10 Hz are required to perform the experiment of mammography at SPARC).

The main challenge regarding the electron beam generation is related to the capability to focus down a high-charge beam (1-2 nC) to focal spot sizes in the order of $10\mu m$ in the collision

point, which in turns implies to accurately take under control emittance and energy spread of the beam itself [15]. The emittance growth is controlled by the emittance compensation method, which is one of the main challenges addressed to the SPARC project. The low energy spread values will be obtained by a proper setting of the injection phases into the accelerating structures, which compensates the linear correlation of the longitudinal phase-space, while, in a second step,the use of an X-band short length RF structure [16] will allow to reach an rms energy spread smaller than 5×10^{-4}. The electron beamline consists in a 30 m double dogleg starting downstream the SPARC photoinjector; it ends in a two branch beam delivery line that provides two separate Interaction Regions with the possibility to host two different experiments at the same time. The total beam deflection is about six meters from the SPARC photoinjector and undulator axes. A total of six 25 degrees dipoles and 20 quadrupoles are needed to drive the electron beam up to the two IRs, their procurement has been finalized in July 2009 and the complete delivery is expected by the end of 2010, together with the related Power Supplies for a total of 26 units.

A normal conducting large solenoid has been chosen as the final focusing element.This will ensure a high field on axis (0.9T), in spite of the wide aperture in the magnet, necessary for the FLAME laser beam to pass through it avoiding interactions with the internal surface of the vacuum chamber. The technical specifications of the solenoid have been finalized in 2009, and the delivery is expected by the end of 2010. In Fig. 9 the a sketch of the final engineered model are shown.

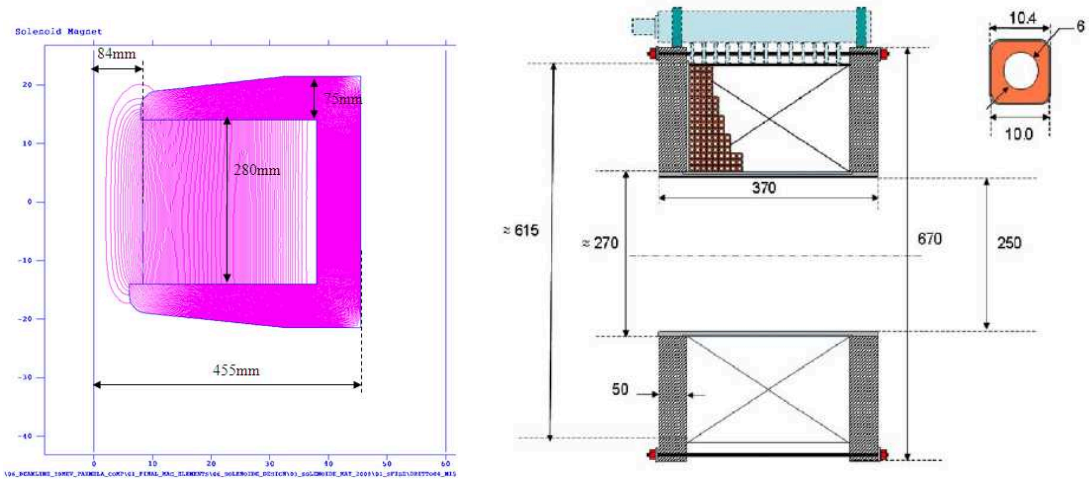

Figure 9: IR solenoid two dimensional profile (left) and enginered model (right).

Also the final dipole meant to dump the electron beam downstream the interaction has been defined; the presence of a high permeability metal shield will prevent the presence of the bipolar field in the interaction point to perturb electrons trajectories. Fig. 10 points out the dipole field profile as modified by the shield, standing to 3D FEM simulations.

The interaction chamber layout has been designed in this year in order to fit all the necessary devices (magnetic elements, optical elements, vacuum vessels, diagnostics, etc.) in agreement with the beams transport constraints. the procurement will be completed in 2010. In this setup the electron beam alignment will be monitored using BPMs and high resolution imaging systems.Time

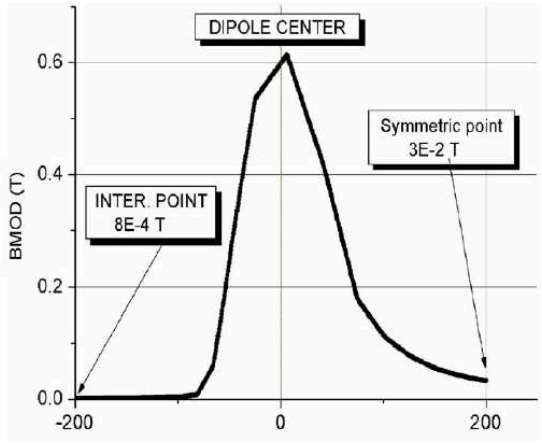

Figure 10: Last dipole field profile.

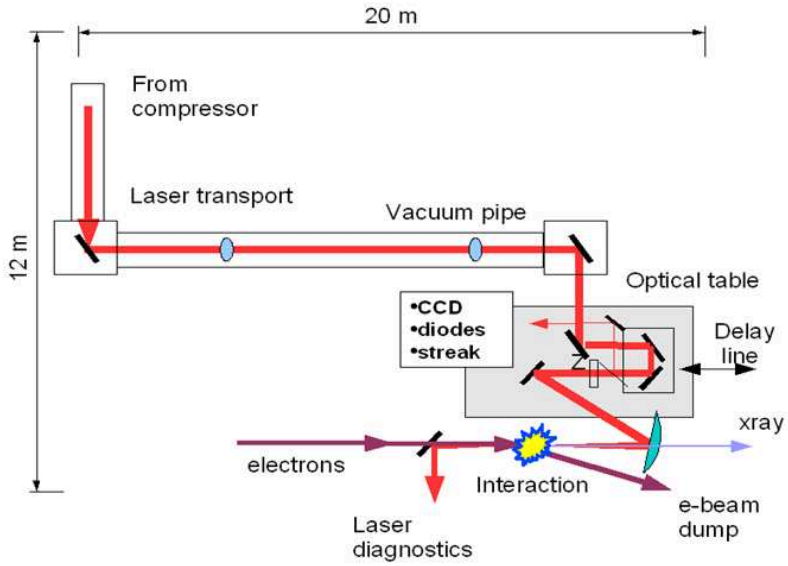

Figure 11: Schematic drawing of the radiation beamline for the Thomson Source.

Table 4: List of expected laser beam parameters.

Parameter	Value
Wavelength(nm)	800
Compressed pulse energy(J)	5
Pulse duration/bandwidth (ps/nm)	$3 \div 12(80)$
Rep.Rate(Hz)	10
Prepulses contrast	$> 10^6$
Contrast ratio at 1 ns before (ASE)	$> 10^8$
Contrast ratioat 1100 ps before	$> 10^6$
Contrast ratio of replica	$> 10^5$
Beam quality M^2	≤ 1.5
Energy stability	10%
Pointing stability (μm)	< 2
Synchronization with SPARC clock	< 1 ps

overlapping between laser pulse and electron beam (in the interaction chamber) will be adjusted using an optical delay line, while jitter/delay readout will be made through a picosecond streak-camera, by monitoring laser and some kind of electron beam induced radiation (e.g.Cherenkov, transition radiation).

5.2 The laser beam transferline

After the compressor, the laser beam will be transported to the experimental chambers through 30 m in vacuum pipe.The beam will be then focused to the interaction point using an off-axis parabola (focal length 75 cm and aperture15 cm). A series of diagnostics, controls and motorized optical elements will be useful tools to optimize the overlapping between the laser and the electron beam. In Fig. 11 a schematic drawing of the radiation beamline is shown, while in table 4 the laser parameters for the Thomson experiment are given.

References

1. L.A. Gizzi et al., Europ. Phys. Journal Special Topics, 175, 3-10 (2009)
2. F. Anelli, A. Bacci, D. Batani, M. Bellaveglia, C. Benedetti, R. Benocci, L. Cacciotti, C.A Cecchetti, O. Ciricosta, A. Clozza, L. Cultrera, G.Di Pirro, N. Drenska, R. Faccini, M. Ferrario, D. Filippetto, S.Fioravanti, A. Gallo, A. Gamucci, G. Gatti, A. Ghigo, A. Giulietti, D. Giulietti, L. A. Gizzi, P. Koester, L. Labate, T. Levato, V. Lollo, E. Pace, N. Pathack, A.R. Rossi, L. Serafini, G. Turchetti, C. Vaccarezza, P. Valente, C. Vicario, *Design of the Test Experiment for the Sub-Pw Flame Laser System at LNF-Frascati: Electron Acceleration with Self-Injection (SITE)*, Unpublished, October 2009.
3. L. A. Gizzi et al., Il Nuovo Cimento C, 32, 433 (2009).
4. A. Pukhov and ter Vehn J., Appl. Phys. B, **74**, 355 (2002).
5. Gordienko S. and Pukhov A., Phys. Plasmas, **12**, 043109 (2005).
6. Lu W. et al., Phys. Rev. Special Topics - Accelerators and Beams, **10**, 061301 (2007).

7. L. A. Gizzi et al., Phys. Rev. E 79, 056405 (2009).

8. C. Benedetti, A. Sgattoni, G. Turchetti and P. Londrillo, IEEE Trans. Plasma Sci., **36**, 1790 (2008).

9. C. Benedetti et al., Nucl. Instr. & Meth. A, **608**, 594 (2009).

10. A.R. Rossi et al., Phys. Rev. S.T.A.B. **12**, 104202 (2009).

11. A.G. Argentieri et al., Nucl. Instr. & Meth. A (2009).

12. G. Mazzitelli et al., Nucl. Instr. & Meth. A **515**, 524 (2003).

13. A. Bacci et al., Nucl. Instr. & Meth., doi:10.1016/j.nima.2009.05.041 (2009).

14. U. Bottigli et al., Il Nuovo Cimento, **29C**, N.2 , Marzo Aprile 2006.

15. W.J. Brown et al., Phys. Rev. STAB **7**, 060702 (2004).

16. D. Alesini et al., Nucl. Instr. & Meth. A **586**, (2008).

From LNF-INFN report 2010

NTA-PLASMONX

S. Bellucci, S. Bini, M. Castellano, A. Clozza, G. Di Pirro, A. Drago,
M. Esposito, M. Ferrario, A. Gallo, G. Gatti, P. Gaudio, A. Ghigo,
G. Giannini, T. Levato*, F. Micciulla, M. Migliorati, D. Nanni,
E. Pace, L. Palumbo, A. Petrucci, C. Sanelli, A. Tenore,
F. Terra, S. Tomassini, C. Vaccarezza (Resp.)

In collaboration with:
Sezione INFN Bologna, Sezione INFN Milano, Sezione INFN Milano Bicocca,
Intense Laser Irradiation Laboratory, INO-CNR and Sezione INFN Pisa,
Universitá La Sapienza, Roma

* also at ILIL, INO-CNR, Pisa, Italy

1 Introduction

In the 2010 the NTA-PLASMONX project has seen the completion of FLAME-laboratory that was officially opened in December. The commissioning activity has been carried on through all the year and also the Self Injection Test Experiment has completed its first phase. The MultiGev spectrometer has seen the completion of the prototype tests and the detector has been constructed and assembled, its commissioning also started. The electron beam transfer lines for the Thomson Scattering and Plasma Acceleration experiments are going to be installed in the mid of 2011, being the procurement of all components finalized for that date. The Thomson source interaction setup will also be installed together with the setup of the BEATS2 experiment. The description of this activity is given in the following.

2 FLAME and SITE

During 2010 the main part of the FLAME laboratory was completed including the laser area, the target area, the beam transport and most of the radiation protection shielding. This activity culminated in the Official opening which took place during the LIFE meeting at LNF on Dec. 17th. In section 2.1 of this report we describe in details the commissioning activity and the series of tests carried out including sub-system tests and full system test with laser power up to 50 TW in the target chamber. In Section 2.2 we describe the outcome of the preliminary phase of the Self Injection Test Experiment (SITE) [1]. Here a list of the main data concerning the entire Laboratory with some specification on the first test on instrumentations including the auxiliary (probe) and main laser beams.

2.1 FLAME LASER OPERATION

During 2010 all subsystems of the laser, namely the front-end, the 10 pumping units of the main cryo amplifier, the beam transport, the optical compressor vacuum chamber and the compressor optics were commissioned and successfully tested. In particular, during specific test runs a full beam compression test was carried out in March 2010 in which a pulse duration of 26 fs was demonstrated for the main beam and 23 fs for the aux beam (see Fig. 1). In addition, in April 2010, the contrast of the laser pulse at a TW power level was measured, demonstrating the expected contrast ratio of better than 109 as shown by the plot of Fig. 2.

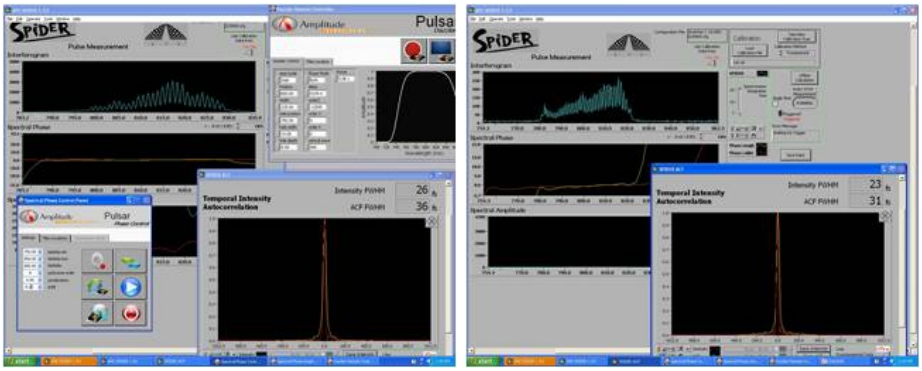

Figure 1: *User interface of the Dazzler-Mazzler control showing optimized pulse duration of 26 fs for the main pulse (left) and 23 fs for the the auxiliary (probe) pulse (right).*

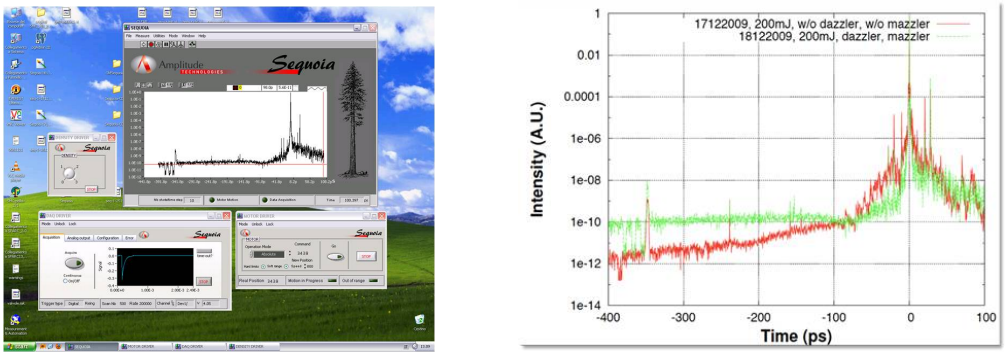

Figure 2: *(Left) User interface of the Sequoia cross-correlator during contrast measurements at FLAME. (Right) Plot of the cross-correlation curve with and without pulse duration optimization showing an optimum contrast of better than* 10^{10}.

2.1.1 FLAME Target Area shielding

During May 2010, the vertical radiation shield was completed to enable full shielding of the target vacuum chamber. The shielding consists of concrete blocks of 50 cm thickness held together by a state-of-the-art steel frame. During the following month, the horizontal shielding, consisting of 50 cm thick, "T" shaped, concrete beams was also commissioned. These shielding structures, together with the additional labyrinth vertical shielding planned in 2011 (see general FLAME plan on 2009 report [2]) will provides full protection against ionizing radiation generated in laser-plasma acceleration interaction conditions [3] as from SITE design [4] (Fig.3).

2.1.2 Beam transport and pointing stability test

During June 2010, full commissioning took place of the beam transport line from the laser clean room (laser output) to the target chamber, via the in-vacuum optical compressor and turning mirrors. This also included the installation of the 1m focal length off-axis parabolic mirror (OAP) for beam focusing at the target vacuum chamber center. Beam pointing stability tests were carried out to evaluate overall pointing performance including intrinsic laser pointing stability and transport line mechanical stability. The final result is shown in Fig.4 where the focal spot image taken

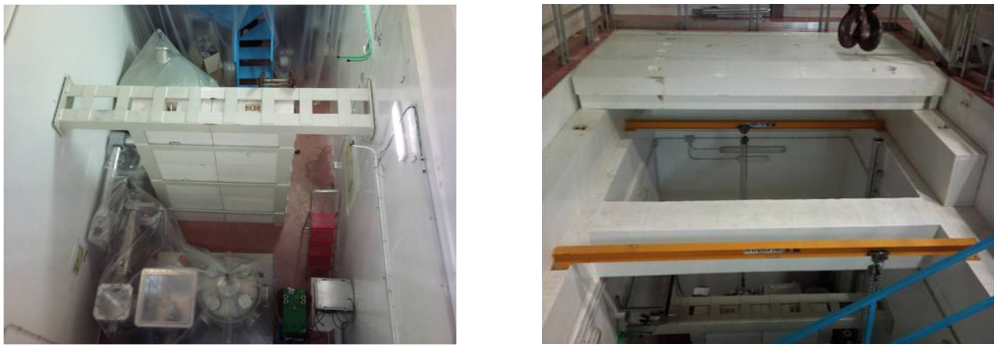

Figure 3: *Vertical (left) and horizontal (right) concrete shielding for the underground FLAME target area were the test esperiment of laser-plasma acceleration with self-injection takes place.*

with a 20x microscope objective is shown along with the statistical distribution of the centroid of the focal spot in the X and y directions. According to these measurements an excellent pointing stability of better than $2\mu rad$ is found, which is a small fraction of the focal spot itself.

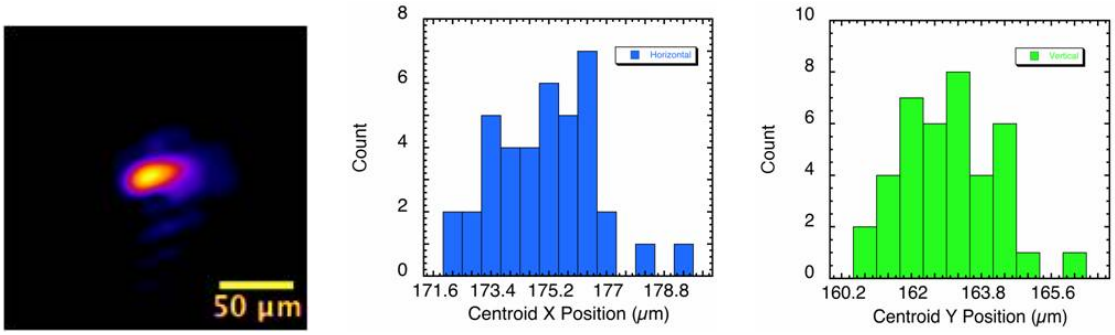

Figure 4: *Beam pointing stability at target chamber center. Left image shows the focal spot image taken with a 20x microscope objective. Centre and right images show the statistical distribution of the centroid of the focal spot in the X and y directions.*

For the optimization of the off-axis parabola, in addition to standard alignment procedures, an additional alignment procedure previously used and tested at ILIL, was established at FLAME. The procedure is based upon the optimization of the forward scattered radiation from laser interaction in air at relatively low laser power. Due to interaction of the laser pulse with the air gases, a self-phase modulation occurs along with harmonic generation. A symmetric image (see figure 5) is indicative of a well optimized focal spot, with a minimum astigmatism.

2.1.3 Gas-jet installation and tests

During July 2010 the gas-jet system including the nozzle and the valve, the high pressure gas system and the XYZ micrometric target motion mechanism were fully commissioned and tested. The pictures of Fig. 6 show the entire system (left) and a detail of the nozzle (right) during propagation of the laser pulse in the gas-jet. The latter image was obtained from the Thomson scattering imaging channel which is looking at the target from the top, in the direction perpendicular to the plane of oscillation of the electric field of the laser e.m. wave.

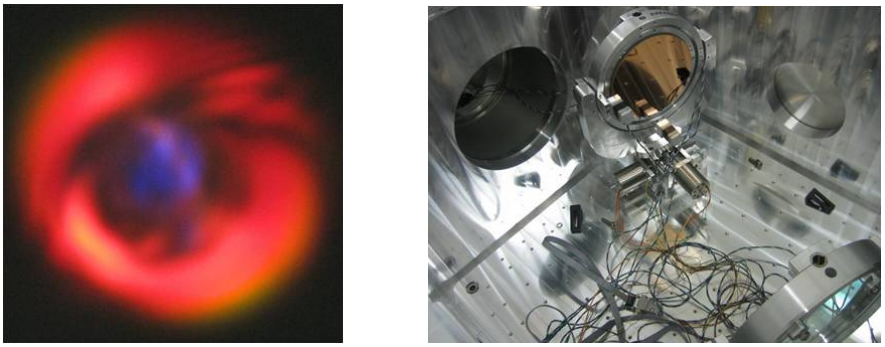

Figure 5: *Beam pointing stability at target chamber center. Left image shows the focal spot image taken with a 20x microscope objective. Center and right images show the statistical distribution of the centroid of the focal spot in the X and y directions.*

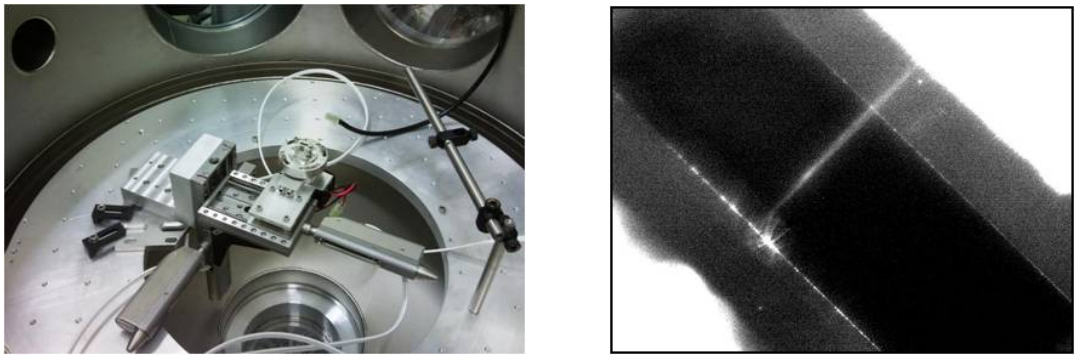

Figure 6: *(Left) Panoramic view of the target motion assembly with XYZ micro metric translation stages. (Right) Magnified top-view of the gas-jet nozzle (gas ejected normal to the image) showing the passage of the laser pulse focused at the center the slit through the gas at low laser power. The width of the nozzle is 1.2 mm.*

2.1.4 *Laser on gas-jet target: first plasma*

Starting from August 2010, a series of tests were carried out to optimize the entire optical system and establish alignment procedures to be used during the SITE experimental phase. These tests culminated with the generation of the first plasma from gas-jet interaction with a 300 mJ level. During this phase a great effort was dedicated to the control of the pulse duration via optimization of the FLAME Dazzler-Mazzler devices for optimization of the bandwidth. These tests enabled the experimental team to gain full control of the procedure and knowledge of the critical parts of the system enabling them to successfully reproduce optimum laser-pulse duration during experimental runs.

2.1.5 *First laser accelerated electron bunches from self-injection*

Starting in September 2010 an intense experimental activity was initiated aimed at finding the conditions for achievement of laser-plasma acceleration with self injection. During this phase, due to safety constraints, the main power amplifier was turned off (no pumping) and the laser output was limited to a few TW. A detailed description of the experimental set up of this phase is given elsewhere ([4] and a more detailed description of the results is given below in the next session. In Fig. 7 we show an example of the first electron bunch obtained on October 6th, as detected from the LANEX screen placed along the path of the accelerated electrons in the direction of propagation of the laser pulse. This result demonstrated that the experimental set up, including main laser and experimental such as pulse compression and beam focusing and target system synchronization, were successfully controlled and that performance of the entire system at this relatively low laser power were within specifications required for laser-plasma acceleration.

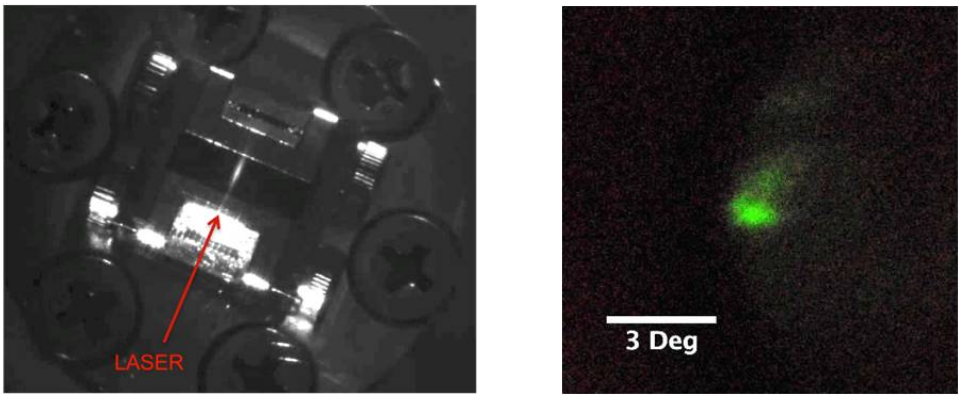

Figure 7: *Left) Top-view of the gas-jet nozzle showing Thomson scattering from the laser-plasma interaction region along the path of the laser pulse at relatively higher power than in the similar image of Fig. 6. (Right) First electron bunch obtained with FLAME on October* 6^{th}*, as detected from the LANEX screen placed along the path of the accelerated electrons in the direction of propagation of the laser pulse.*

2.1.6 *Starting up the main power amplifier*

Immediately after the first successful generation of laser-accelerated electron bunches with self injection, tests began on the optimization of the last power amplifier which culminated with systematic tests of the full energy stability. The plots of Fig 8 (left) show the stability tests of the

energy over a relatively large number of shots. After the entire optimization process, the full laser energy before compression was found to be 7.3 J (Fig. 8 right).

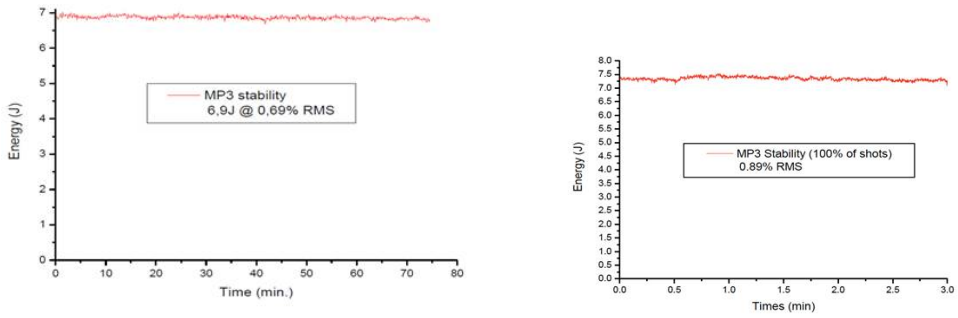

Figure 8: *(Left) Full output energy stability of the laser over a 80 min period showing RMS stability of better than* 1 *at 6.9 J. This level of energy was further increased to 7.3 J after additional optimization.*

2.1.7 Starting up the main power amplifier

As a final step for laser characterization during 2010, wavefront measurement were carried out in view of the planned installation of the adaptive optics planned for 2011. These measurements were carried out before and after the main power amplifier. Measurements before the main amplifier (top of Fig. 9) show a high quality wave front before the main amplifier, with only minor distortions on the edges of the beam and a Strehl ratio of better than 0.9.

The same measurements carried out after the main amplifier (Fig.9 bottom) show a significant increase in the distortions introduced by the main amplifier. In fact, a close look at the expected intensity in the far field (focal spot) shows the presence of a secondary focal spots, containing a significant fraction of the energy with remaining energy filling up the area around these two spots. Further investigation of these issues was carried out by the laser manufacturer and an upgrade of the main amplifier is foreseen during 2011 to mitigate these issues. An almost complete correction of the phase distortion will eventually be carried out using the full aperture adaptive mirror.

2.1.8 Summary of laser performance as end of 2010

Following the results of all the tests carried out on the laser system during 2010 and also taking into account the measurements performed at the target chamber center, the performance of the laser at this stage can be summarized by the table 1.

As compared with the expected performance and in view of the forthcoming planned experimental activity, at this stage we can conclude that, following the installation of the adaptive optics, all laser parameters are expected to be well within required specifications. Currently, the uncorrected wave-front distortion limits the intensity in the focal spot in the present configuration (SITE) to the mid $10^{18} W/cm^2$.

2.2 THE SELF-INJECTION TEST EXPERIMENT(SITE) - Phase 1

As originally planned, the first phase of SITE took place in parallel with the laser optimization to enable assessment of the laser performance and establishment of all procedures, including safety

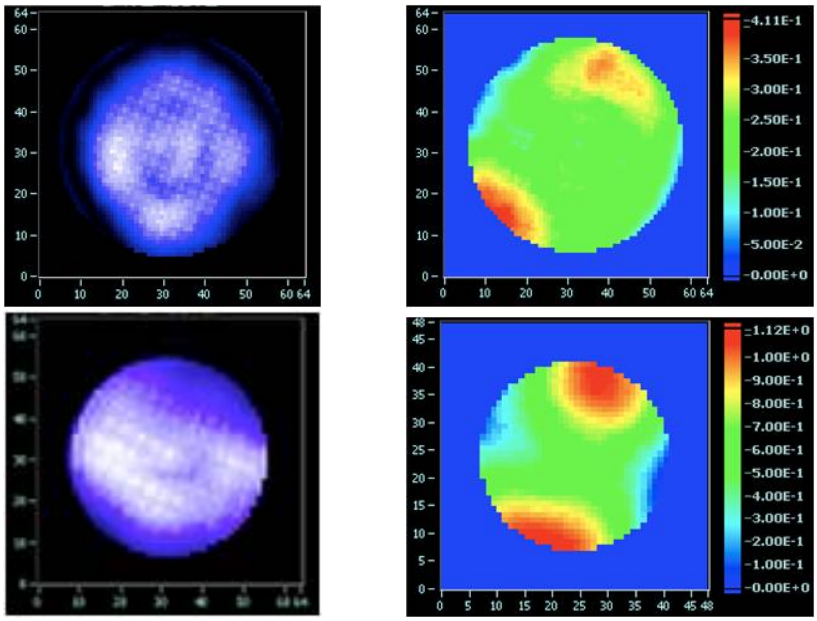

Figure 9: *Wave-front measurements of the FLAME laser pulse showing the intensity (left) and the phase (right) of the beam before (top) and after the main power amplifier (bottom). Analysis of these wave fronts yields a Strehl ratio of 0.9 before the main amplifier.*

Table 1: Summary of FLAME performance.

Energy before compression	$7.3J$
Vacuum compressor transmission	$> 70\%$
Pulse duration down to	$23fs$
ASE Contrast ratio: better than)	$1 > 2 \times 10^9$
Prepulse contrast: better than	10^8
RMS Pulse Stability	$< 0.8\%$
Pointing Stability (incl.path)	$< 2\mu rad$
Phase front correction needed:	adaptive optics
Full power vacuum compression:	to be performed

procedures. SITE - Phase 1 also served for a preliminary assessment of radiation protection measures and, in fact, measurements were carried under the supervision of LNF radiation protection authority.

2.2.1 SITE experimental arrangement

A minimum set of experimental diagnostics was set up to establish key physical parameters, including laser propagation and focusing, target reliability, electron beam production and energy. For these studies we used a nitrogen gas-jet with backing pressure ranging from 5 to 60 Bars. The gas-jet nozzle could be moved with micrometric resolution along the three Cartesian axes. Here we recall the basic experimental set-up schematically shown in the image of Fig. 10 where the gas-jet nozzle is shown with the laser pulse focused close to the edge.

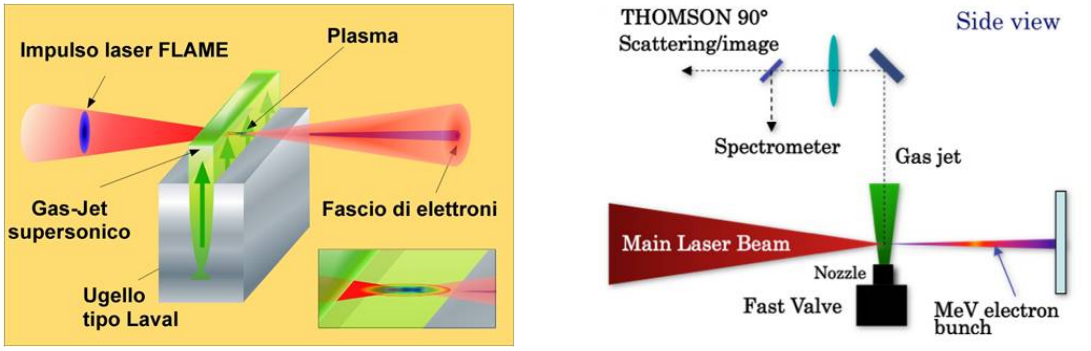

Figure 10: *Schematic experimental set-up for the self-injection test experiment showing the focusing configuration relative to the gas jet nozzle and the main diagnostics for laser, plasma and electron bunch characterization.*

Following the initial successful shots with production of accelerated electron bunches, a more systematic study was carried out aimed at identifying optimum conditions for production of collimated electron bunches of the highest energy for the given laser power. Using available diagnostics, a position scan was carried of the laser focal spot position relative to the gas-jet input wall. For a given longitudinal gas-jet position, a transverse (horizontal and vertical) scanning was also carried out to look for the best injection conditions which, as discussed elsewhere [4], are sensitive to the gas density gradient as well as to the gas absolute density. The latter parameter was scanned by changing the backing pressure of the gas.

2.2.2 Electron bunch collimation study

Initially we looked for the minimum laser energy requirements for electron acceleration, and we found it near the 500 mJ laser output level. In this condition we investigated the forward transmitted optical radiation during gas-jet longitudinal positioning and gas pressure. During this study we found condition in which self-focusing was most likely taking place enabling an acceleration regime similar to the one already explored at ILIL in a previous experimental campaign [5]. The effect of self-focusing was clearly shown by the dramatic change in the spectrum and divergence of the transmitted radiation. This also had a direct effect on the production of energetic electron bunches. In fact, it was possible to identify three different interaction condition for which accelerated electrons were characterized by no collimation, medium (around 30 mrad) and high collimation (around 5 mrad).

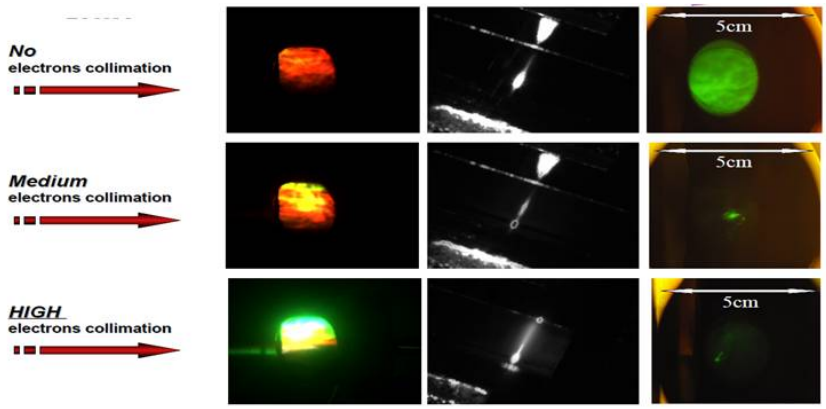

Figure 11: *Raw data from the initial measurements for the SITE Phase 1. The three columns of images show (from the left) the beam after propagation in the plasma, the Thomson scattering image and the electron bunch on the LANEX screen. The upper row shows the interaction regime in which no collimation was found. Middle and bottom show similar results for medium and high degree of electron bunch collimation.*

These three different collimation regimes were observed to be also related to the different spectrum in the transmitted laser radiation as shown in Fig. 11. According to these images, collimation of electrons is reasonably correlated with a longer interaction length in the gas, as shown by the Thomson scattering image. In addition, the transmitted light appears to be strongly blue-shifted when collimation occurs. This is most likely due to the sustained propagation and increased effect of ionization induced blue-shift in the gas.

2.2.3 Collimated bunches: pointing and quality

Following the collimation study presented above, a stable regime of production of collimated bunches could be established at 1 J laser energy. The sequence of LANEX images of Fig. 12 shows a sample of the data in which electron bunches in the range between 5 and 30 mrad were systematically accelerated. In this interaction regime, a first investigation was also carried out on the role of the front-phase distortion and consequent spot size energy distribution with related effect on accelerated electron bunch.

Once this condition was established, data were also taken at higher laser energy, up to the maximum of 2.5 J before compression. These additional measurements enabled us to identify the role of phase front distortions in the quality of accelerated electron bunches. In fact, further increasing the laser energy to the multi-Joule level (less than 2.5 J) showed the effect of the secondary focal spot in the interaction region, as discussed above in Section 2.1.8. Fig. 13 presents the LANEX data (top) which clearly show the production of a double electron bunch structure. The corresponding Thomson scattering images (bottom row of Fig. 13) consistently show a double propagation channel. Indeed, these results seem to confirm the presence of a double focal spot in the interaction region as obtained from the wave-front analysis discussed above. This effect only appears at a relatively high energy level when the secondary focal spot contains a sufficient level of energy resulting, in some case, in a second accelerated bunch. A detailed analysis of this effect is in progress [6].

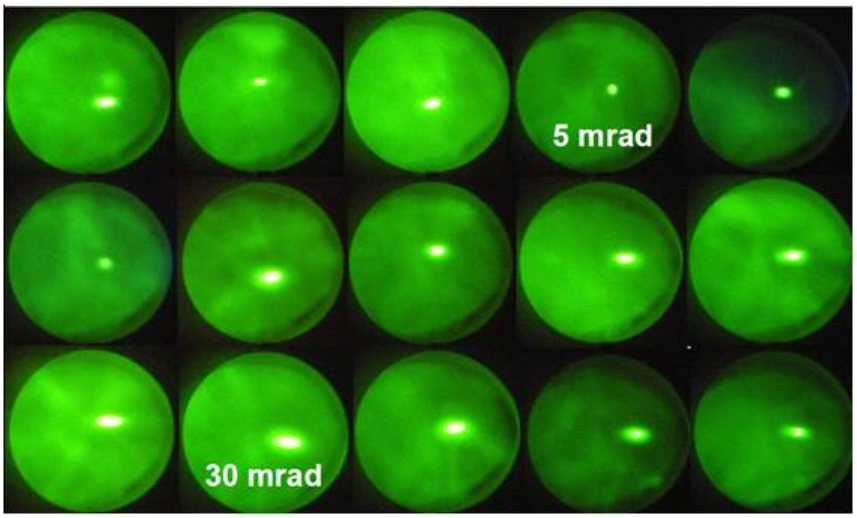

Figure 12: *Raw LANEX data showing the production of collimated electron bunches in the range of 5 to 30 mrad.*

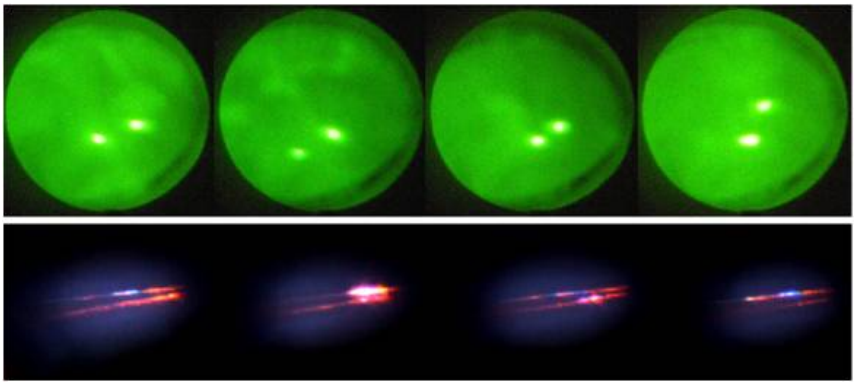

Figure 13: *Raw LANEX data (top) showing the production of a double electron bunch structure. The corresponding Thomson scattering images (bottom) consistently show a double propagation channel.*

2.2.4 *Collimated bunches: electron energy*

As discussed in the dedicated section below, a high resolution magnetic electron spectrometer was undergoing commissioning during 2010. During this preliminary SITE - Phase 1 measurements, the activity of the magnetic spectrometer was devoted mainly to calibration and noise reduction. In spite of this, a successful preliminary energy measurement was also obtained ad described in the spectrometer section below. Here we report on the results obtained initially with a stack of radiochromic films as described in [7], see Fig. 14. Preliminary analysis of SHEEBA measurements confirmed that the energy of electron accelerated at 1J level laser energy were already in the 50 MeV level. Following these preliminary encouraging measurements, we also used a low resolution magnetic spectrometer built using a 1T permanent magnets and a LANEX screen as shown schematically in Fig. 15.

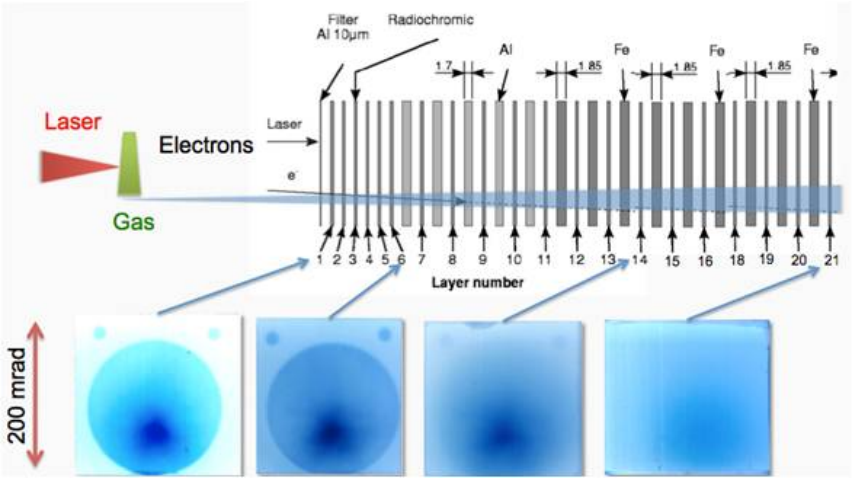

Figure 14: *Raw data from preliminary energy measurements of the accelerated electron bunches obtained using a stack of radiochromic films configured according to [7]. Data were obtained after integration over 31 shots.*

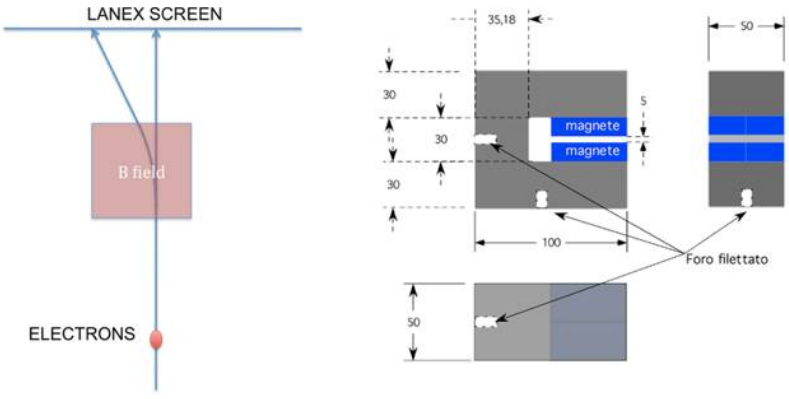

Figure 15: *Schematic of the low-resolution permanent magnet electron spectrometer.*

In this way it was possible to observe the main feature of the accelerated electrons increasing

the laser energy at fixed pulse duration and focal spot. Preliminary analysis of the low resolution spectra show clearly that high collimated and high energetic electron bunches (around 5 mrad and over 200 MeV level) was accelerated. Although more accurate measurements are still needed to confirm these preliminary, we can conclude that SITE-Phase 1 measurements fully succeeded in demonstrating activation of high energy laser-plasma electron acceleration with self-injection at FLAME in the multi-hundred MeV range. This is extremely encouraging in view of the ultimate goal of the SITE which, as described in details [4], aims at delivering stable production of 1 GeV class electron bunches with moderate-to-small energy spread.

3 The Multi-GeV Electron Spectrometer

As far as the electron spectrometer [8] is concerned, during the year 2010 three man activities have taken place: the studies on the prototype have been finalized, the detector has been constructed and assembled and the commissioning of the detector on the final environment has started. The prototype is made of 64 1mm fibers coupled with the same readout chain as the detector 16. It has been tested on the SPARC THz line and at BTF. The major problem that had to be faced was a saturation effect induced by the extremely large number of photons produced in the fibers. To avoid saturation of the electronics readout the HV supplied to the photomultipliers (PMT) was reduced down to typically 500V from the 900V nominal value. A trickier saturation effect was although observed in the tests on beam: the signal shape resembled the beam profile, but the integral of the observed signal was independent of the total impinging charge (see figure 17). This was due to a saturation of the anodic current and was cured by attenuating the light on the photocathode with optical filters.

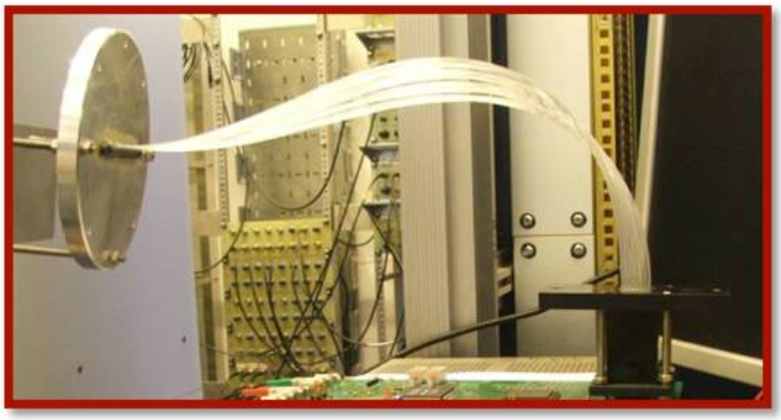

Figure 16: *Prototype of the fiber detector of the electron spectrometer of SITE.*

After fixing this problem we could calibrate the detector response in charge utilizing the variable charge of the BTF beam. There is still a saturation effect but it starts when more than a hundred of nC impacts a set of 64 fibers, condition that should not occur in the final experimantal setup (Fig. 18).

During 2010 the construction of the detector was completed, with the realization of the vacuum chamber equipped with fibers, the assembly of the photomultipliers and the electronics. The final detector is shown in figure 19.

To complete the assembly of the detector, each PMT mask was aligned at the sub-millimiter level to reduce the effect of cross talk.

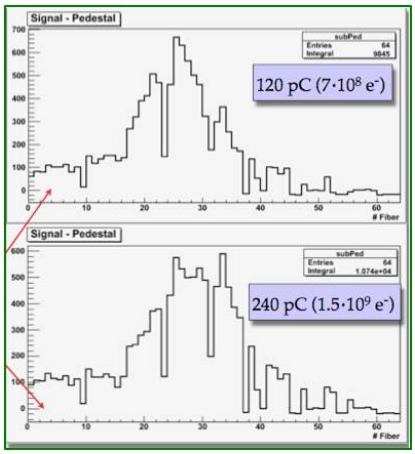

Figure 17: *Saturation effect: measured spectra of the BTF beam. Note missing variation with increasing charge.*

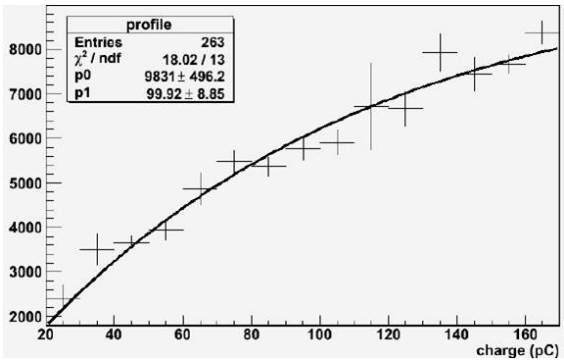

Figure 18: *Calibration curve of the fiber detector of the electron spectrometer of SITE.*

Figure 19: *The Magnetic Spectrometer of SITE.*

Finally in november 2010 two days of shots of FLAME with the target where devoted to the commissioning of the spectrometer. The first tests showed a huge electromagnetic noise induced by the interaction of the laser with the plasma. It was found to have contributions from several sources: it was picked up both by the PMT and by the cables and could be screened by moivng the detector behind the wall. While prolongations of the fibers are being built a temporary solution to the problem was found by reading the PMTs with cameras. After running the resulting images through the standard reconstruction algorithms, the spectra in Fig. 20 (taken under different conditions than the ones previously shown) were observed, thous demonstrating that the rest of the measurement chain works.

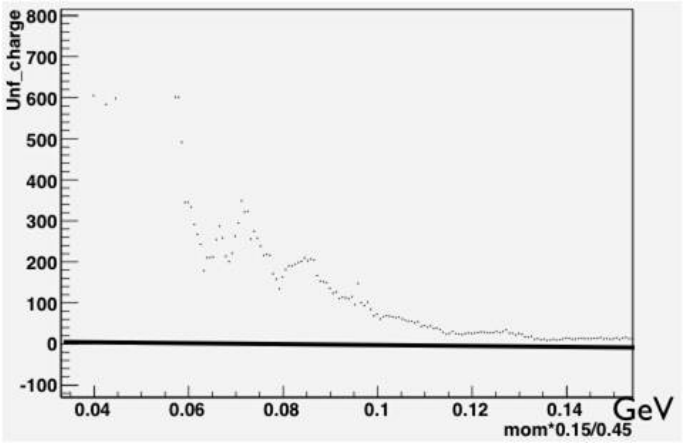

Figure 20: *First electron spectrum from Laser-Plasma acceleration coming from the magnetic spectrometer of SITE.*

4 The Thomson Source

In this facility several experiments are foreseen such as high gradient plasma acceleration and the production of monochromatic ultra-fast X-ray pulses by Thomson back-scattering(TS). The TS X-ray source [9] will be the first one to be installed and its main features are flexibility and potential compactness with respect to conventional synchrotron sources. A TS source driven by high-quality electron beams can work in different operating modes, e.g.: the high-flux- moderate-monochromaticity-mode(HFM2) suitable for medical imaging when high-flux sources are needed; the moderate-flux- monochromatic-mode(MFM) suitable to improve the detection/ dose performance [10]; short-and-monochromatic-mode(SM) useful for pump-and-probe experiments e.g. in physical-chemistry when tens of femtosecond long monochromatic pulses are needed.

4.1 Electron beamlines

The electron beamlines design has been completed in 2009, with the capability to transport electron beams with energies ranging from 28 MeV up to150 MeV in two separate interaction points (IP's). The goal of the electron beam transport is to preserve the high brightness coming from the linac and to ensuring a very tight focusing for the whole energy span. The final features that the electron beam will show at the two interaction points, are reported in Table 2. The general layout has been revised in the last months of 2010 in order to accomplish the conventional safety requirements: basically the two interaction points have been switched in order to provide a suitable high energy

diagnostic line for the plasma accelerated electron beam while keeping a proper free way out from the SPARC hall in the two ways as required from the conventional safety system. The new all view of the PLASMONX beam lines within the SPARC hall is showed in Fig. 21.

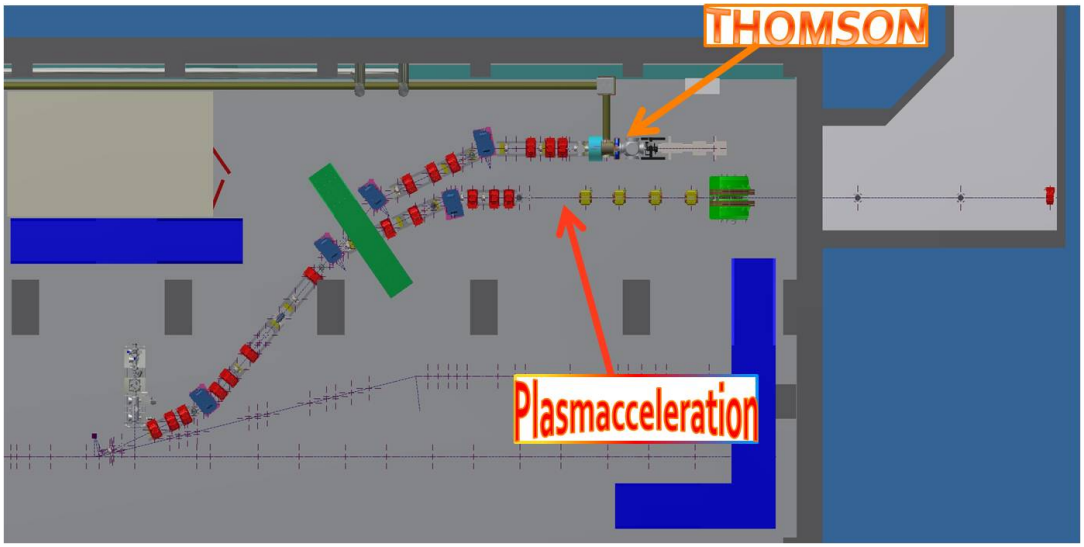

Figure 21: *Updated lay-out of the dog-leg like electron beamline for the PlasmonX experimental area.*

In detail the electron beamline consists in a 30 m double dogleg starting downstream the SPARC photoinjector; it ends in a two branch beam delivery line that provides two separate interaction regions with the possibility to host two different experiments at the same time. The total beam deflection is about six meters from the SPARC photoinjector and undulator axes. A total of six 25 degrees dipoles and 20 quadrupoles are needed to drive the electron beam up to the two IPs, their procurement has been finalized in July 2009 and the complete delivery is expected by summer 2011, together with the related Power Supplies for a total of 26 units. The installation will begin in July and is foreseen to end in September 2011. The commissioning will follow right after.

After the layout update the beam dynamics for the electron beam has been checked to ensure the all the required parameters reported in Table 2 are still valid. Three main cases have been addressed in term of electron beam transverse dimensions at the IP's, emittance dilution due to Coherent Synchrotron Radiation, final energy spread and longitudinal dimension:

- a) 30-150 MeV beam for Thomson scattering experiment
- b): 150 MeV for Plasma Acceleration experiment

As an example for the Thomson scattering experiment the main challenge regarding the electron beam generation is related to the capability to focus down a high-charge beam (1-2 nC) to focal spot sizes in the order of $10\mu m$ in the collision point, which in turns implies to accurately take under control emittance and energy spread of the beam itself [11]. The emittance growth is controlled by the emittance compensation method, which is one of the main challenges addressed to the SPARC project. The low energy spread values will be obtained by a proper setting of the injection phases into the accelerating structures, which compensates the linear correlation of the longitudinal phase-space, while, in a second step,the use of an X-band short length RF structure [12]

will allow to reach an rms energy spread smaller than 5×10^{-4}. A normal conducting large solenoid provides the final focusing element at the IP that will see the first experiment to be set up. The soleonid will ensure a high field on axis (0.9T), its technical specifications have been finalized in 2009, and the delivery is expected by the summer of 2011.

In Fig. 22 the transverse beam rms size evolution is reported for the Thomson scattering setup starting from the photoinjector down to the IP as obtained from the simulations performed with the Tstep code tracking 15 kparticles, for a beam energy of 30 meV (BEATS2 experiment), i.e. where th space charge effects are still important. The same is provided in Fig. 23 where the beam energy instead is around 150 MeV and the simulatiions performed with the Elegant code and about 120kparticles.

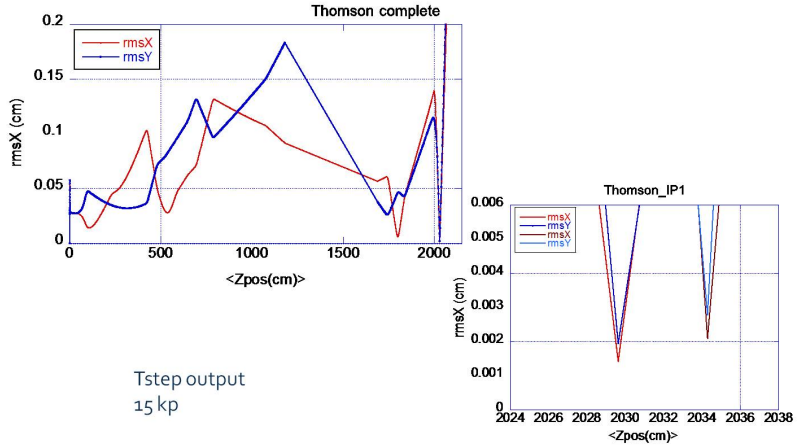

Figure 22: *Rms beam sizes eveolution along the transfer line (left), and detail of longitudinal "tunability" of the beam waist at the interaction point.*

In Fig. 24 the 3D drawing of the whole interaction chamber is shown as embedded in the solenoid and dumping dipole field, together with the parabolic mirror that focuses the laser beam coming from Flame on the interaction point. The interaction chamber layout has been designed in order to fit all the necessary devices (magnetic elements, optical elements, vacuum vessels, diagnostics, etc.) in agreement with the beams transport constraints, its delivery is foreseen in summer 2011.

The electron beam alignment will be monitored using BPMs and high resolution imaging systems. The time overlapping between laser pulse and electron beam (in the interaction chamber) will be adjusted using an optical delay line, while jitter/delay readout will be made through a picosecond streak-camera, by monitoring laser and some kind of electron beam induced radiation

Table 2: *Electron beam parameters at the two interaction points.*

Parameter	Thomson Scattering Exp.	Plasma Acceleration Exp.
Bunch charge(nC)	$1 \div 2$	0.020
Energy (MeV)	$28 \div 150$	150
Length (ps)	$15 \div 20$	0.010
$\epsilon_{nx,y}$ (mm-mrad)	$1 \div 5$	$1 \div 0.5$
Energy spread(%)	$0.05^{1} \div 0.2$	0.01
Spot size at interaction point rms (mm)	$5 \div 10$	$5 \div 10$

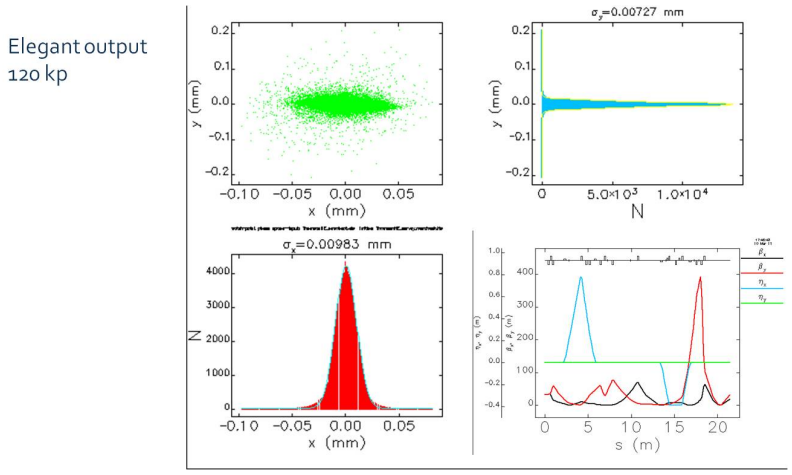

Figure 23: *Rms beam sizes of the 150 MeV beam at the interaction point, together with the twiss parameters for the transfer line (down right).*

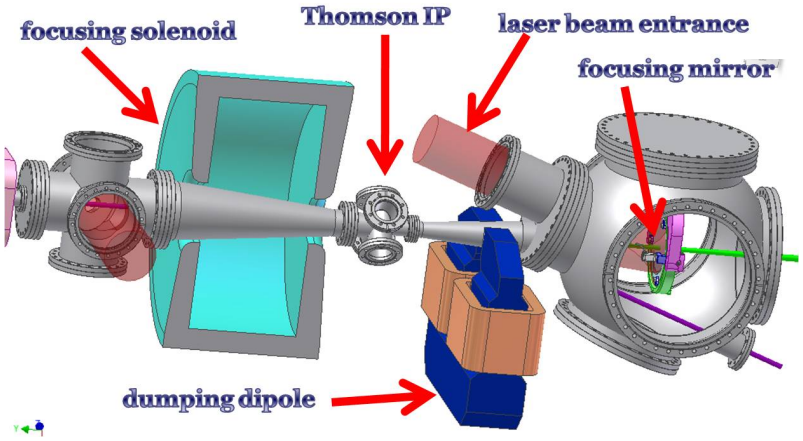

Figure 24: *3-D schematic layout of the Thomson scattering interaction chamber.*

(e.g.Cherenkov, transition radiation).

For the experiment of plasma acceleration the electron beam transport tracking has been also performed with Elegant checking the feasibililty of the parameter list reported in Table 2, the results are shown in Fig. 25 and 26.

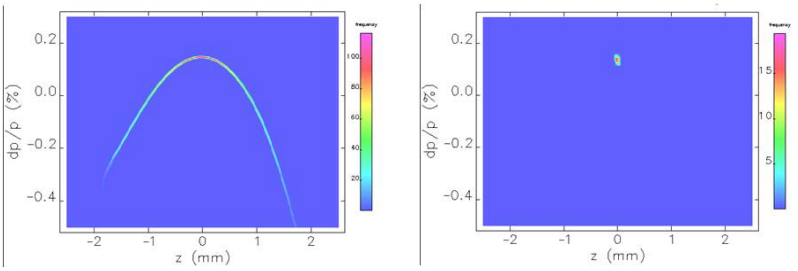

Figure 25: *Longitudinal distribution of the electron beam at the exit of the photoinjector (left), and at the plasma acceleration interaction point.*

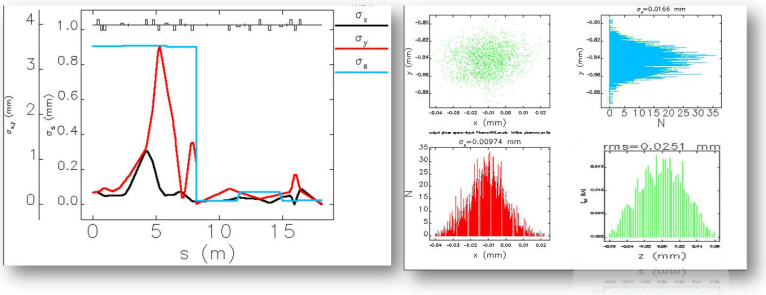

Figure 26: *Evolution of the rms electron beam sizes along the trasnfer line (left) and at the interaction point (right).*

4.2 The laser beam transferline

The laser beam transfer line to the interaction region is composed by a series of high reflectivity mirrors installed in a vacuum pipe 50 m long. The mirrors, 8 inches diameter, will be supported by motorized gimbal mounts in order to assure the alignment to the off-axis parabola that focus the laser pulse on the electron beam. The design of the line has been performed with ZEMAX optical code to simulate the effect of the misalignment of the mirrors on the final spot.The coating of the individual mirror has been choosen with the best reflectivity at the work polarization that change because of the beam trajectory. All the components of the lines: mirrors, gimbal mounts, vacuum chambers, pumps etc. have been ordered.

Table 3: *List of expected laser beam parameters.*

Parameter	Value
Wavelength(nm)	800
Compressed pulse energy(J)	5
Pulse duration/bandwidth (ps/nm)	$3 \div 12(80)$
Rep.Rate(Hz)	10
Prepulses contrast	$> 10^6$
Contrast ratio at 1 ns before (ASE)	$> 10^8$
Contrast ratioat 1100 ps before	$> 10^6$
Contrast ratio of replica	$> 10^5$
Beam quality M^2	≤ 1.5
Energy stability	10%
Pointing stability (μm)	< 2
Synchronization with SPARC clock	< 1 ps

References

1. L. A. Gizzi *et al.*, Il Nuovo Cimento C, **32**, 433 (2009).
2. S. Bellucci *et al.*, NTA PlasmonX, on "Annual Activity Report 2009", (2010).
3. L. A. Gizzi, E. Clark, D. Neely, L. Roso, and M. Tolley, "High repetition rate laser systems: targets, diagnostics and radiation protection" AIP Conf. Proc. The 2nd International Conference on UltraIntense Laser Interaction Science, Vol. 1209, pp. 134-143, February 2, 2010 doi:10.1063/1.3326308
4. F. Anelli *et al.*, "Design of the Test Experiment for the Sub-Petawatt Flame Laser System at LNF-Frascati: Electron Acceleration with Self-Injection (SITE)", Unpublished, October 2009.
5. L. A. Gizzi *et al.*, "Laser-Plasma Acceleration: First Experimental Results from the Plasmon-X Project", Proceedings of the 51st Workshop of the CHANNELING 2008 Conference on "Charged and Neutral Particles Channeling Phenomena", World Scientific Publishing, The Science and Culture Series - Physics, pp. 495-501, (2010), ISBN:978-981-4307-00-0.
6. L.A. Gizzi *et al.*, Abstract, Plasma Physics Conference, European Physical Society, 2011.
7. M. Galimberti, A. Giulietti, D. Giulietti, L.A. Gizzi, Rev. Sci. Instrum. **76**, 053303 (2005).
8. R. Faccini *et al.*, Nucl. Instr. & Meth. A **623**, 704 (2010).
9. P. Oliva *et al.*, Nucl. Instr . & Meth. A **615** 93, (2010).
10. U. Bottigli, *et al.*, Il Nuovo Cimento **29C**, N.2 , Marzo Aprile 2006.
11. W.J. Brown *et al.*, Phys. Rev. STAB **7** (2004) 060702
12. D. Alesini *et al.*, Nucl. Instr. & Meth. A **586** (2008) 133.

From LNF-INFN report 2011

NTA-PLASMONX

M. Bellaveglia, S. Bellucci, S. Bini, M. Castellano, E. Chiadroni, A. Clozza, L. Coderoni, G. Di Pirro, A. Drago,
M. Esposito, M. Ferrario, D. Fililppetto, A. Gallo, C. Gatti, G. Gatti, P. Gaudio, A. Ghigo, G. Giannini, T. Levato*, F. Micciulla, M. Migliorati, A. Mostacci, D. Nanni, E. Pace, L. Palumbo, A. Petrucci, I. Sacco, C. Sanelli, A. Tenore, F. Terra, S. Tomassini, C. Vaccarezza, C. Vicario
Laboratori Nazionali di Frascati

C. Benedetti, G. Turchetti
Sezione INFN Bologna

A. L. Bacci, F. Broggi, M.M. Cola, A. Flacco, C. Maroli, M. Passoni, V. Petrillo, N. Piovella, R. Pozzoli, M. Romé, A. R. Rossi, L. Serafini
Sezione INFN Milano

D. Batani, R. Benocci
Sezione INFN Milano Bicocca

C.A.Cecchetti, A.Gamucci, D.Giulietti, L.A.Gizzi, L.Labate, N.Pathak, F. Piastra
Intense Laser Irradiation Laboratory, INO-CNR and Sezione INFN, Pisa

N. Drenska, R. Faccini, P. Valente
Dip. Fisica Univ. La Sapienza, Roma

* also at ILIL, INO-CNR, Pisa, Italy

1 Introduction

In the 2011 the NTA-PLASMONX project has seen the completion of FLAME-laboratory and the successful first experimental champaign in November on self-injection laser plasma electron acceleration at low laser power (10TW). The commissioning activity has been carried on through all the year and also the Self Injection Test Experiment has completed its first phase. The SITE spectrometer activity has seen in this year the development of full MC simulation together with the study of electronic noise remedies and the development of an alternative readout based on optical devices, Also the design and the acquisition process for the high energy version of the spectrometer magnet have been completed. The installation of the electron beam transfer lines for the Thomson Scattering and Plasma Acceleration experiments have been carried on during 2011. The Thomson source interaction final setup will take place on spring 2012 together with the setup of the BEATS2 experiment. The description of this activity is given in the following.

2 FLAME commissioning

During 2011, the FLAME system was fully commissioned with complete hardware installation and extensive performance tests. Special attention was devoted to the performance of the system at full energy. During this year a full training was performed to LNF personnel by the Pisa group to transfer the expertise on any system and subsystem of the Flame Lab, inclusing the laser and the target area. This training, starting from the control of the laser system parameters up to the high power is currently going toward the new experimental phase where the strong collaboration between this two groups on the Laser from one side and the Laser-Plasma interaction from the other will be essential to reach the final goal consisting in GeV level electron acceleration by plasma

wave.
A detailed description of the laser system was already given in the previous report. Here we summarize the system specifications and focus on final performance completed on Dec. 2011. The FLAME Amplitude laser is based upon Ti:Sa, chirped pulse amplification (CPA) system that will deliver 25 fs, 800 nm, up to 220 TW, laser pulses with a 10 Hz repetition rate at a fundamental wavelength of 800 nm. The system features a high, sub-ns contrast ratio ($> 10^{10}$) and has a fully remotely controlled operation mode. The system includes a front-end with pulse contrast enhancement (booster), bandwidth control and regenerative amplifier and yields pulses with 0.7 mJ in 80 nm bandwidth. These pulses are then further amplified by the first amplifier to the 25 mJ level while the second amplifier brings the energy to the 600 mJ level. The third cryogenic amplifier (MP3) is based upon a 50 mm Ti:Sa crystal pumped by 10, frequency doubled Nd:YAG laser pulses for a total of up to 20 J of energy at 532 nm. The extraction energy is as high as 35%, leading to a final energy in the stretched pulses in excess of 7 J. The typical spectrum of the pulse at the exit of MP3 and the stability of the output energy are shown in Fig.1.

As anticipated above, major effort was dedicated during the final phase of the commissioning, to the characterization of the main parameters at full energy.

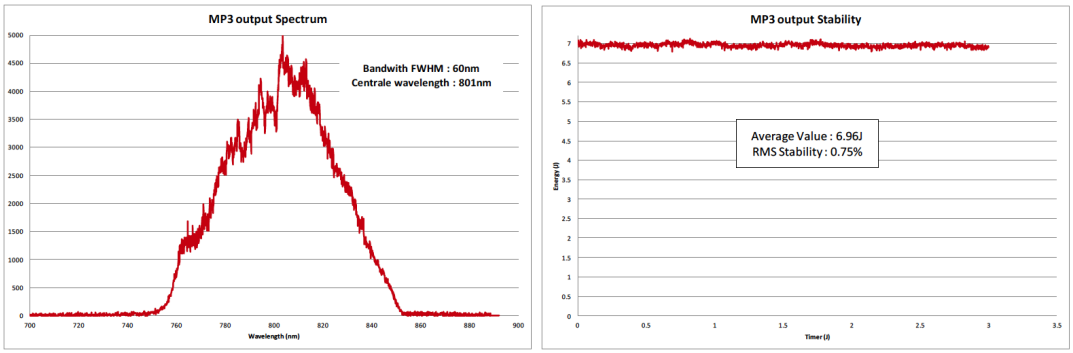

Figure 1: (left)Typical spectrum of the laser pulse at the exit of the power amplifier(MP3) and (right) measurement of the stability of the output energy at close to maximum pumping level.

Pulses at the output of MP3 are then transported in air to the vacuum compressor placed in the underground target area. At the entrance of the compressor the beam pattern, as obtained with the "burn paper" technique, is shown in Fig.2.

The pulse is then compressed to a minimum pulse duration below 30 fs, as shown by the Fig.**??**. Once compressed, the pulse in transported under vacuum to the target chamber via remotely controlled beam steering mirrors. The plot of Fig. 3 shows the cross correlation curve of the FLAME laser system showing the level of ASE just above 10^{-9} of the peak intensity.

This value of the ASE laser contrast is well above the typical value usually found in multi-stage Ti:Sa laser systems in which the typical laser contrast does not exceed 10^7. In the typical experimental conditions of laser wakefield acceleration with self-injection, the laser pulse is focused at peak intensities exceeding 10^{18} W/cm^2 which, with our ASE contrast, gives a precursor laser intensity on target below 10^9 W/cm^2. In the case of interaction with gases with pressures ranging from 1 to 10 bar, this laser intensity is below the plasma formation threshold for laser pulses of sub-nanosecond duration [**?**] which is the typical duration of ASE pulses. Therefore we can reasonably assume that in the cse of interaction with gases, no premature plasma formation occurs and the CPA pulse can be focused directly in the gas. However, according to the cross-correlation curve of Fig. 3 (right) some precursor radiation may be present on the ps time scale before the pulse reaches the peak intensity. This radiation may give rise to premature ionization of the

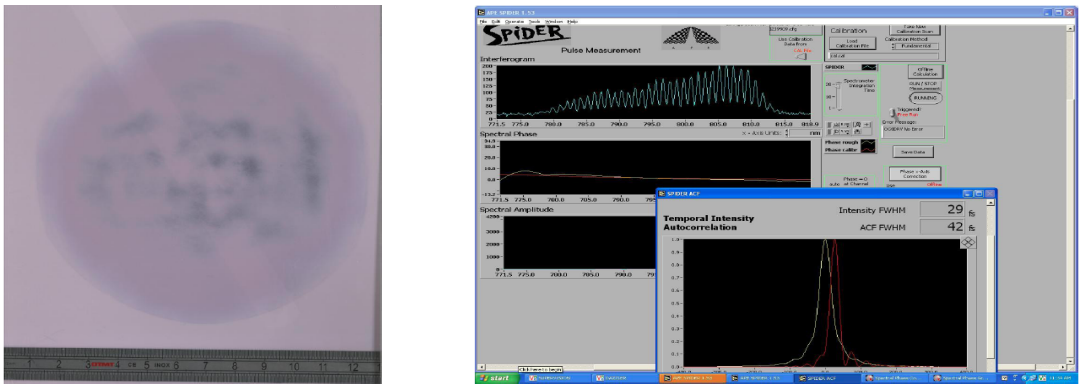

Figure 2: (left)Pattern of the beam intensity at 4.6 J pulse energy, taken at the entrance of the vacuum compressor and (right) pulse duration measurement carried out using the Spider technique

gas. A quantitative analysis of this ionization process will be the subject of investigation of the interferometric measurements which, as discussed below, will rely on femtosecond-scale resolution capability.

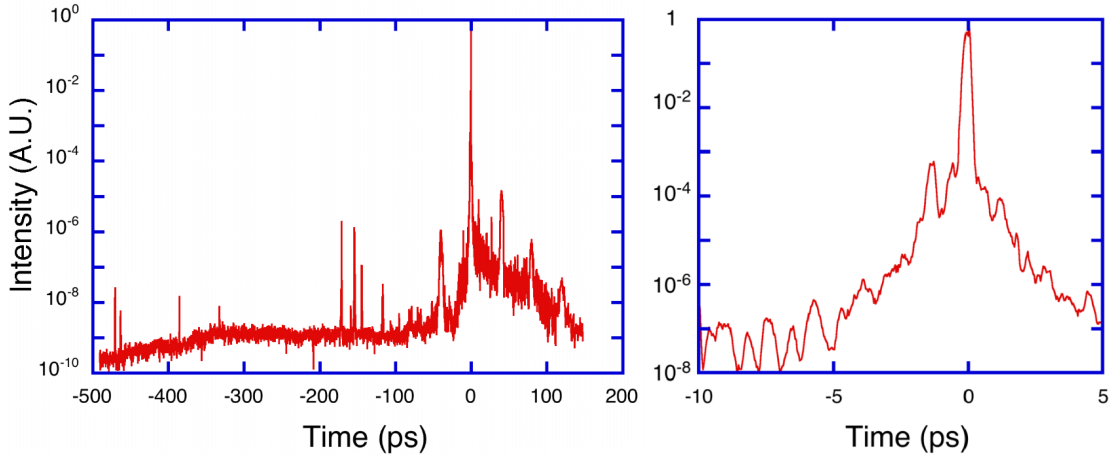

Figure 3: Cross-correlation curve (left) showing the detailed temporal structure of the laser pulse in the 500 ps window before the main pulse. The plot on the left shows that intensity of the amplified spontaneous emission is just above 10^{-9} of the peak intensity. The plot on the right shows the detail of the curve in the ps domain, just before the peak intensity.

Special attention was dedicated to the study of the transverse beam profile, using phase and intensity measurements to evaluate the effective Strehl ratio, i.e. the ratio between the energy in the focal spot and the total energy in the pulse. In fact, the beam quality plays a key role in the control of the quality of the bunches in laser wakefield acceleration. Leading research on self-injection now points at the control of the self-injection process as the key to a high quality and reproducible acceleration. At the same time, the higher power that will be available with systems currently under construction, will enable the parameters of self-injection to move towards higher energy and even more stable and higher bunch quality. Among the different uses of FLAME, the scientific programme of the self-injection experiment (SL-SITE) includes the demonstration

of self-injection operations at full laser energy, including optimized phase front corrections. To this purpose, a careful characterisation of FLAME performances, with particular reference to the transverse beam quality was carried out during the commissioning week. The images of Fig. 4 show the measured intensity and the phase of the beam (near field) and the focal spot (far field) calculated using the measured intensity and phase.

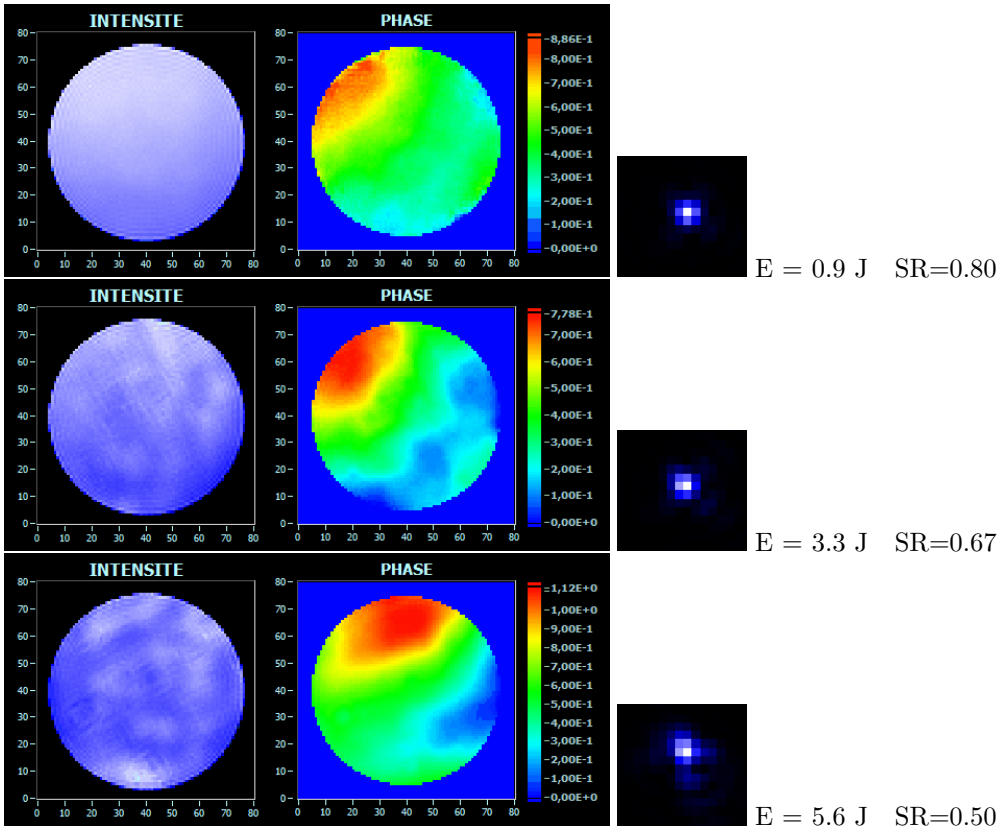

Figure 4: Intensity and phase distribution of the FLAME beam. The Sequence of images shows the the behaviour at increasing laser energy up to the maximum of 7J. The corresponding calculated focal spot intensity is also shown for each frame (right).

According to these results the measured Strehl ratio is greater than 50% up to pulse energies of approximately 6J. For energies between 6 and 7 J, the phase front distortion increases leading to a reduction of the Strehl ratio decreases to a minimum value of 35%. However, our measurements show that the phase front pattern remains very stable from shot to shot at a given pulse energy. This makes the phase front correction with adaptive optics (planned for installation during 2012) a reliable and complete solution to achieve a high quality focal spot.

3 The SITE Spectrometer

During 2011 the activity concerning the electron spectrometer developed along three different lines: development of full MC simulation, study electronic noise remedies, development of an alternative readout based on optical devices, and the design and acquisition of the magnet for the high energy version of the spectrometer itself.

3.1 Full MC

Previous simulations of the expected output of the spectrometer started from a parametrized version of the laser-plasma interactions output and was based on a numerical integration of the equations of motion. We were therefore not sensitive to the low energy tails and to possible scattering on the harware sorrounding the detector (e.g. the magnet)During 2011 a full detector simulation based on GEANT and including both the magnet, the beam-pipe and the supports was setup. Input to this simulation is the output of the PIC simulations so that the effect of low energy or high divergence particles could be estimated. The expected spectrum, compare with the true one is shown in Fig. 5 on the left.

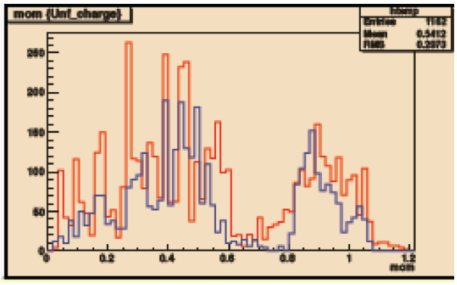

Figure 5: Comparison between the simulated true energy spectrum and the reconstructed one after 50 iterations of the bayesian unfolding.

3.2 Noise fighting

The first electron bunches accelerated with low laser intensity and preliminarly experimental condition in Nov. 2010 showed that the readout electronics suffers from the electromagnetic noise induced by the pulsed high energy field generated in the laser-plasma interaction, making it impossible to discriminate signal from noise. It is worth to stress once again that this was the first attempt of using a not purely optical device in a laser-plasma interaction environment. The most challenging part of the system is indeed the use of photodetectors in a high-noise environment, with both electromagnetic shots and bursts of Xrays directly on multi-pixel photomultipliers.

To reduce the noise the following measures have been taken:

- extend fiber length from 1 to 5 meter, in order to place PMTs and electronics behind the radiation protection wall of the experimental area. The increasing of light attenuation is also an advantage to avoid saturation effects;
- attenuate the signal at the entrance of the Maroc2 chips with customed attenuators realized by the INFN-Roma electronics shop; besides the need to interface the chip with the micro-coaxial cables, the challenging part was to build a device which does not alter the working point of the MAROC chips
- improve the grounding of the whole system
- realize better Faraday cages for screening the PMTs and electronics. The electronics and the PMTs are currently shielded by anodized aluminium, but a μ metal shielding might be required.

This improvements will be tested as soon as the commissioning resumes.

3.3 Optical readout

An alternative and complementary readout system has been set up using 5 digital cameras, each mounted on a metallic support and pointing toward the end of each group of fibers. The cameras are fixed to slide-plates provided with a system of micrometic screws for adjusting the orientation of the support plane (left panel of figure 6). The cameras are operated in a triggered mode. The trigger signal, synchronous with the laser-pulse arrival, is received from a socket located on the back of the housing. The data is then transmitted via ethernet to a dedicated computer.

The data coming from the cameras consist of 8-bit images of the scintillation light exiting the fibres, and has to be converted to a series of numbers representing the light output of each channel. This is done by summing the pixel values of all images of the fibers. The fiber positions in an image are determined by constructing grids on calibration images with a dedicated VI (a LabView program), as shown in the right panel of figure 6. Using these grids a raw spectrum is obtained for each camera image and the output is written to a binary file (figure 7).

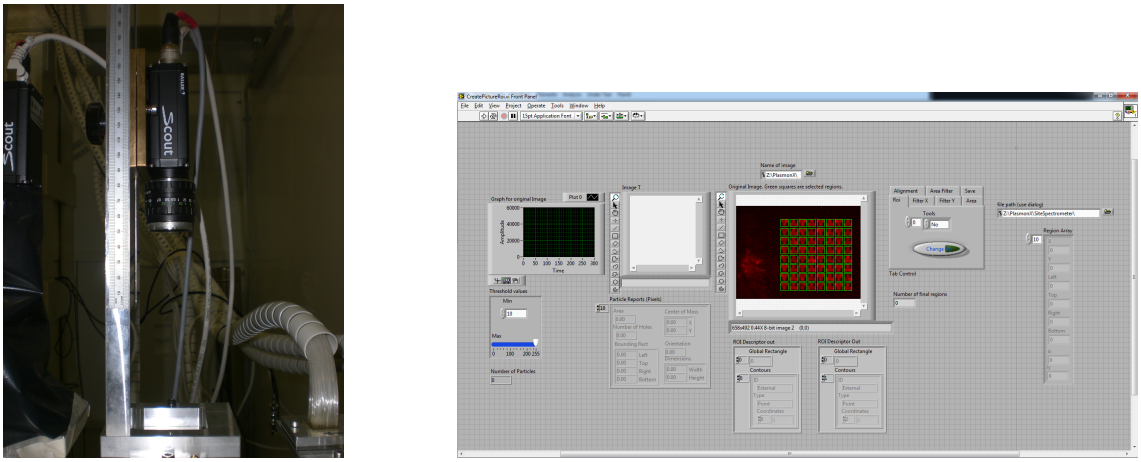

Figure 6: Left:Picture of a camera mounted on the metal support pointing to the fiber matrix. Right: Picture of the LabView Panel of the VI used for identifying the 64 channels from a calibration image obtained with the digital camera.

3.4 Event display and online analysis

Binary files written from photomultiplier readout-electronics and/or from digital-camera DAQ-system are read, eventually in a combined way, and analized online with a dedicated VI. The VI front panel, shown in figure 8, displays raw data (top left), pedestal-subtracted data (bottom left) and unfolded momentum distributions (top right).

3.5 Magnet upgrade

The ultimate goal of the device is to achieve an energy resolution better than 1% at energies as high as 1 GeV and to be sensitive in the multi-GeV regime. To this aim a brand new magnet, with a magnetic length twice as big as the current one and a magnetic field in the plateaux region of more than 1.5T is required. A 3D simulation of the magnetic field and an initial dimensioning of the system has been carried out during 2011, that lead to the issuing of a bid to identify the best

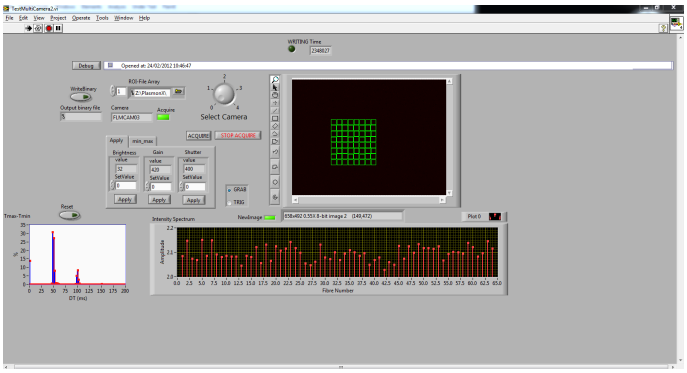

Figure 7: DAQ panel showing the grid used for summing the pixel values of the acquired image and the corresponding raw spectrum.

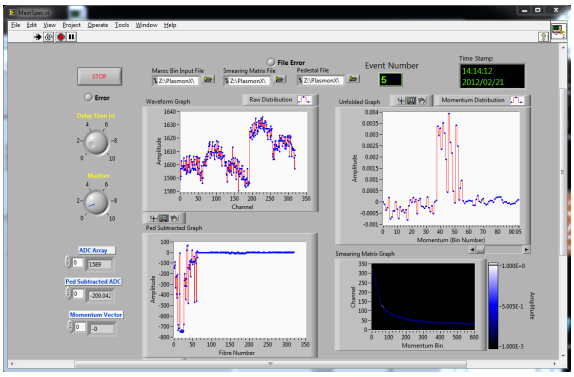

Figure 8: Front panel of the online-monitor VI, showing raw data (top left), pedestal-subtracted data (bottom left) and unfolded momentum distributions (top right).

provider of such a magnet. The expected performances of the spectrometer after the upgrade are shown in Fig. 9 on the right. The bid will close in March 2012.

4 The Thomson Source

The PlasmonX project foresees two kind of experiments such as high gradient plasma acceleration and the production of monochromatic ultra-fast X-ray pulses by Thomson back-scattering(TS). The TS X-ray source [10] will be the first one to be installed and hereby will be described in deeper detail; the key point of the its configuration are the flexibility and the potential compactness with respect to conventional synchrotron sources.
A TS source driven by high-quality electron beams can work in different operating modes, e.g.: the high-flux- moderate-monochromaticity-mode(HFM2) suitable for medical imaging when high-flux sources are needed; the moderate-flux- monochromatic-mode(MFM) suitable to improve the detection/dose performance [11, 12]; short-and-monochromatic-mode (SM) useful for pump-and-probe experiments e.g. in physical-chemistry when tens of femtosecond long monochromatic pulses are needed.

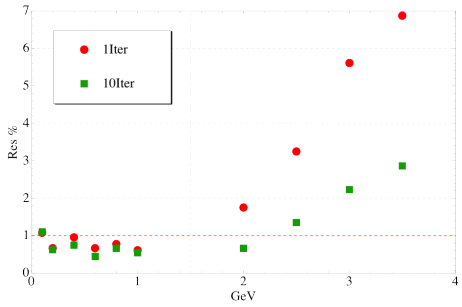

Figure 9: Expected energy resolution with the upgraded magnet.

4.1 Electron beamlines

In 2011 the installation of the PLASMONX beamlines has been almost completed: a twofold transfer line for the electron beam together with a photon beamline that brings the laser pulse from FLAME to the interaction with the SPARC beam. In this configuration the electron beam energy can range from 28 MeV up to 150 MeV, and the electron beam transport is meant to preserve the high brightness coming from the linac and to ensure a very tight focusing and a longitudinal phase space optimization for the whole energy span. The electron beam parameter list for the two interaction points are reported in Table 1. The general layout is showed in Fig. 10, where the PLASMONX electron transfer line departs from a three way vacuum chamber inside the first dipole downstream the RF deflector that is used for the six-dimensional phase space analysis of the SPARC beam. This dipole is also part of the chicane foreseen for the seeding configuration of the SPARC FEL undulator (straight direction downstream the photoinjector) and of the 14 degrees dogleg that brings the electron beam up to the SPARC Therahertz source, see Fig. 11.

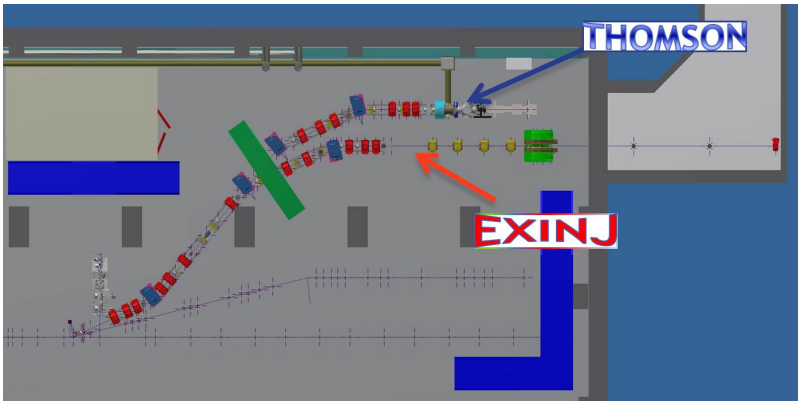

Figure 10: *CAD drawing of the PlasmonX electron beam transfer lines layout.*

The PlasmonX electron beamline consists in a 30 m double dogleg starting, as mentioned, downstream the SPARC photoinjector; they ends in a two branch beam delivery line that provides two separate interaction regions with the possibility to host two different experiments at the same time. The total beam deflection is about six meters from the SPARC photoinjector and undulator axes. A total of six rectangular dipoles and 19 quadrupoles (Fig. 12) are needed to drive the electron beam up to the two IPs, all of them have been installed in autumn 2011 see Fig. 13.

According to the specifications all the magnets have been characterized at the factory mea-

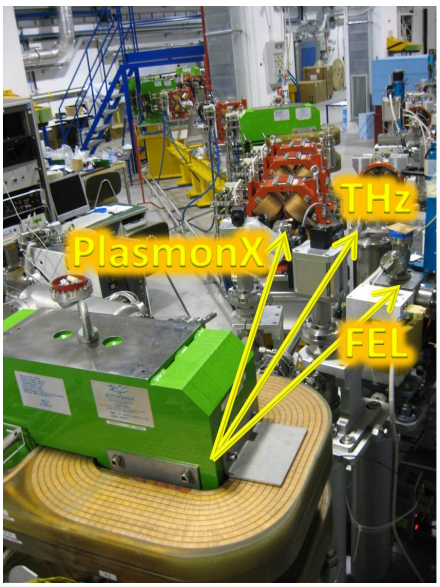

Figure 11: *Three-way branch for the FEL, THZ and PlasmonX beamlines.*

Table 1: Electron beam parameters at the two interaction points.

Parameter	Thomson Scattering Exp.	Plasma Acceleration Exp.
Bunch charge(nC)	$0.2 \div 1.0$	$0.005 \div 0.020$
Energy (MeV)	$28 \div 150$	150
Length (ps)	$15 \div 20$	0.010
$\epsilon_{nx,y}$ (mm-mrad)	$1 \div 5$	$1 \div 0.5$
Energy spread(%)	$0.1 \div 0.2$	0.01
Spot size at interaction point rms (mm)	$5 \div 10$	$5 \div 10$

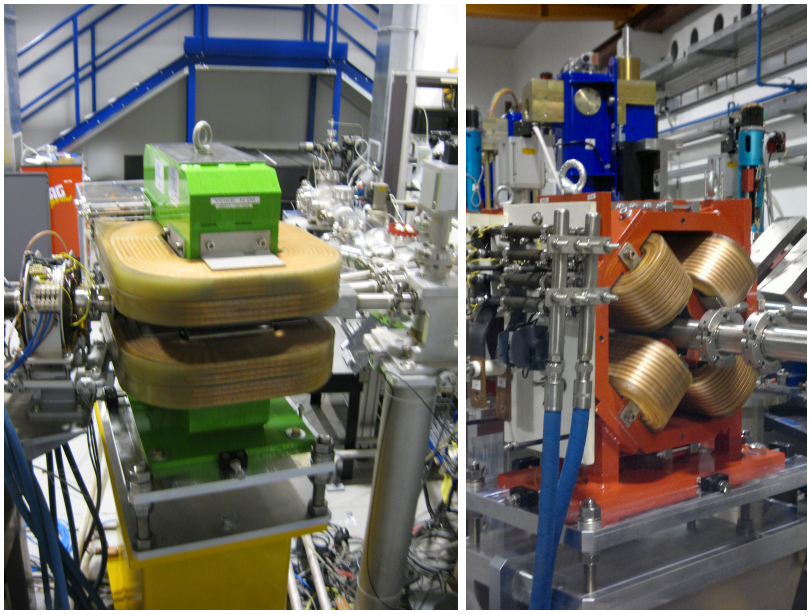

Figure 12: *Dipole (left) and Quadrupole (right) magnets of the PlasmonX electron beamlines.*

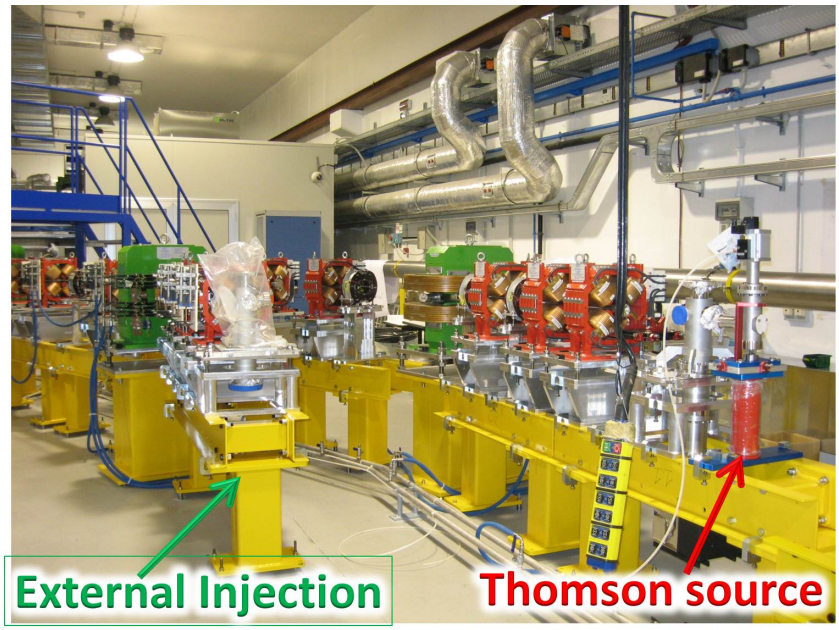

Figure 13: *Final part of the Plasmonx electron beam transfer lines up to the two interaction points.*

suring the magnetic field as a function of the position of a Hall probe inside the magnet poles. As a result at the nominal current all the dipoles show a relative magnetic length deviation of $\sim 0.1\%$ and $\sim 1\%$ from the Tosca 3D code exit value as reported in Fig. 14 while the good field region of $\pm$ 1 cm in both x and y directions shows a maximum deviation of 3×10^{-4}, see Fig. 15.

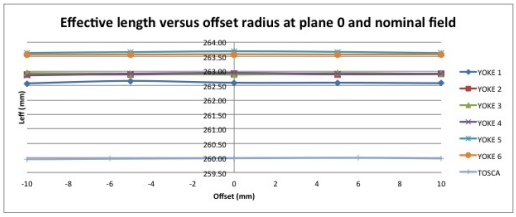

Figure 14: *The effective length of the six dipoles as a result of the magnetic measurements performed with the Hall probe at at the nominal current compared with Tosca code predicted value*

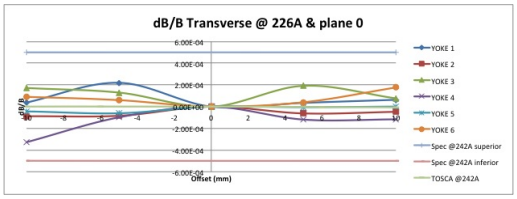

Figure 15: *Measured dipole magnetic field relative deviation vs hall probe position inside the pole expansion.*

The magnetic field quadrupole magnets has been also measured by means of a rotating coil in order to determine the value of the harmonic components up the 20^{th} order and to identify the position of the magnetic axes with the respect of the quadrupole fiducials. In Fig. 16 the relative deviation of the quadrupole gradient is plotted vs the distance from the quadrupole center. After the preliminary alignment performed during the installation of the magnetic elements, a second fine positioning of the magnets will be performed in Spring 2012 to align the magnetic axes on the beam reference trajectory with a resolution of about $50\mu m$.

In place of the foreseen dumping dipole that will be ready at the end of 2012 an existing dipole will be used to dump the electron beam inside the well off in the floor of the hall, this will limit at the beginning the beam energy up to 90 MeV for the 2012 PlasmonX beam experiment. Nine over a total of thirteen Beam Position Monitors are foreseen for the first phase of the Thomson beamline commissioning, together with three high resolution beam imaging setup they will provide the necessary beam diagnostic for the orbit correction and beam phase space measurements. At the beginning the BPM signals will be read by four single pass processors and multiplexed in order to get the whole electron beam orbit readout. By April 2012 the Thomson Interaction vacuum chamber will be delivered, see Fig. 17; the setup consist in two mirror stations that will determine the in & out trajectory of the photon beam, plus an interaction chamber in the middle that hosts the diagnostic for both the electron and photon beams. The parabolic mirror located downstream the interaction point will focuse the photon beam at the IP down to a $10\mu m$ spot size, its spatial adjustment is obtained with its x-y movable support that can be also remotely controlled. The real interaction chamber is a tee-vacuum chamber where a double screen movement will be mounted to get the imaging of the electron and photon beam at the IP.

4.2 The laser beam transferline

The laser beam transfer line to the interaction region is composed by a series of high reflectivity mirrors inserted in a vacuum pipe 50 m long. The mirrors, 8 inches diameter, are supported by motorized gimbal mounts in order to assure the alignment up to to the off-axis parabola that focus the laser pulse on the electron beam. The design of the line has been performed with ZEMAX optical code to simulate the effect of the misalignment of the mirrors on the final spot. In 2011 the installation has been almost completed as shown in Fig. 18: the FLAME laser beam is extracted

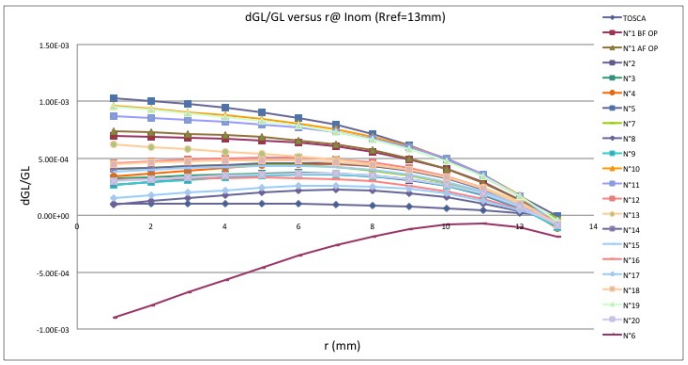

Figure 16: *Relative deviation of the quadrupole gradient plotted vs the distance from the quadrupole center for each of the quadrupole magnet of the transfer lines.*

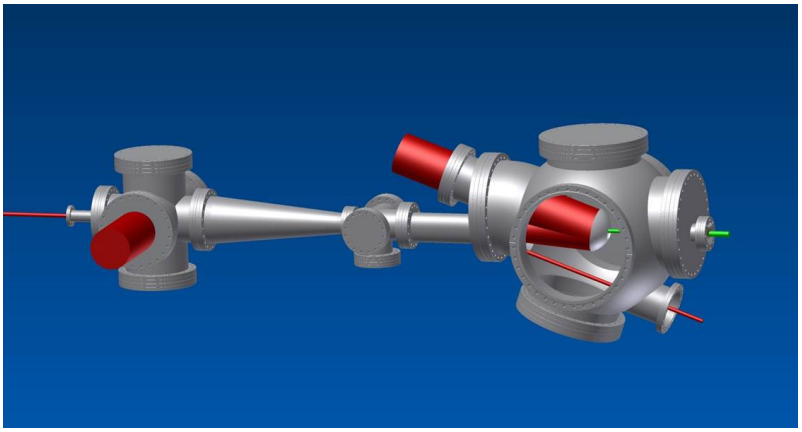

Figure 17: *3-D final drawing of the Thomson scattering interaction chamber*

from the FLAME target area and then guided up to the Thomson IP. A concrete wall has been realized in order to stop any radiation draft from he FLAME area towards the SPARC bunker, and to allow people entering in the SPARC hall during the FLAME laser operation and viceversa, see Fig. 19. The vacuum of the photon beam line is a the level of $10^{-6}Torr$ and suitable for the transport of the compressed laser pulse ($\sim 10fs$ length) as needed for the plasma acceleration experiment. In Table 2 the laser pulse parameters are reported as foreseen for the Thomson Source application.

Table 2: List of expected laser beam parameters.

Parameter	Value
Wavelength(nm)	800
Compressed pulse energy(J)	5
Pulse duration/bandwidth (ps/nm)	$3 \div 12(80)$
Rep.Rate(Hz)	10
Prepulses contrast	$> 10^6$
Contrast ratio at 1 ns before (ASE)	$> 10^8$
Contrast ratioat 1100 ps before	$> 10^6$
Contrast ratio of replica	$> 10^5$
Beam quality M^2	≤ 1.5
Energy stability	10%
Pointing stability (μm)	< 2
Synchronization with SPARC clock	< 1 ps

4.3 The synchronization system

The Thomson scattering experiment needs an extremely precise synchronization between electron bunch and laser pulse. The relative time of arrival jitter of the two beams is fundamental to obtain a repeatable and efficient interaction. The electrons and photons have to be synchronized with a relative jitter $< 500fs$. This can be obtained with a standard electrical distribution of the reference signal, already present at SPARC. Anyway an optical distribution is preferable to obtain precise time of arrival measurement resolution (equal or less than 5fs) and to obtain better synchronization between the two beams. This can be achieved by means of an optical cross-correlation between short laser pulses (100200fs). In particular the electrical (or optical) master oscillator in our project will serve two laser oscillator clients: SPARC photo injector for the production of electrons and FLAME laser for the production of the high intensity pulse for the Thomson interaction.
The RF system phase will be also locked to the master oscillator using low noise phase detection; and the phase feedback loops will be implemented too. They can be divided in two general types: slow (bandwidth $< 10Hz$) and fast (10Hz to some MHz bandwidth). The formers are used typically to compensate slow drifts caused by thermal elongation of cables and are implemented by means of high resolution stepper motors. The others are designed to compensate the high frequency noise suffered by the systems that is normally due to mechanical vibrations or electrical noise in the RF circuits or power amplifiers (klystron tubes and driver amplifiers).

4.4 Beam Dynamics

For the commissioning of the Thomson source that is foreseen to start in April 2012 two working points, WP's, have been studied in view also of the first experiment, BEATS2, requirements:

- a)WP1 that foresees a 350pC beam at the energy of 30 MeV, that will be focused at the IP by means of the final quadrupole triplet only.
- b)WP2 that by using a 1.2 Tesla solenoid will reach the tight focusing of the beam with higher charge up to $Q = 350 \div 1nC$.

In the photoinjctor the emittance growth is controlled by the emittance compensation method [9,11], which is one of the main challenges addressed to the SPARC project. The low energy spread values, $\approx 10^{-3}$ will be obtained by a proper setting of the injection phases into the accelerating structures, which compensates the linear correlation of the longitudinal phase-space. In Fig. 20 the transverse beam rms size evolution is plotted for the Thomson scattering setup starting from the photoinjector down to the IP as obtained from the simulations performed with the Tstep code tracking 15 kparticles, for a beam energy of 30 meV (BEATS2 experiment) and a charge $Q \sim 300pC$. With the only triplet focusing a minimum of $\sigma_{x,y} \approx 50\mu m$ is obtained from simulations (WP1 setup). According to simulations the same beam can be focused down to $\sigma_{x,y} \approx 10\mu m$using the normal conducting large solenoid to provide a field on axis of about 0.9T. The delivery is expected by Fall 2012.

Figure 18: *Plasmonx laser transferlines inside the SPARC bunker (left). Motorized mirror vacuum chamber. (right)*

References

1. L. A. Gizzi, F. Anelli, C. Benedetti, C. A. Cecchetti, A. Clozza, G. Di Pirro, N. Drenska, R. Faccini, D. Giulietti, D. Filippetto, S. Fioravanti, A. Gamucci, L. Labate, T. Levato, V. Lollo, P. Londrillo, E. Pace, G. Turchetti, C. Vaccarezza, P. Valente and C. Vicario, Laser-plasma acceleration with self-injection: A test experiment for the sub-PW FLAME laser system at LNF-Frascati, Il Nuovo Cimento C, **32**, 433 (2009)

Figure 19: *Concrete labirinth wall realized in front of the FLAME to SPARC bunker laser beam access, for shielding radiation (left). On the right a detail of the wall connection between the two experimental areas*

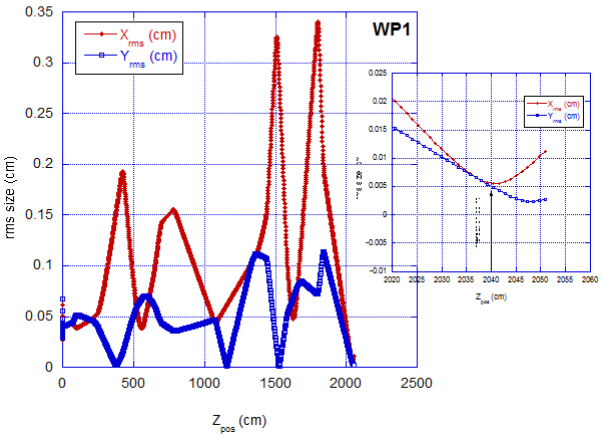

Figure 20: *Evolution of the rms electron beam sizes along the trasnfer line (left) and at the interaction point (right) for the WP1 working point, i.e.* $Q \approx 300pC$ *and with only the final triplet focusing.*

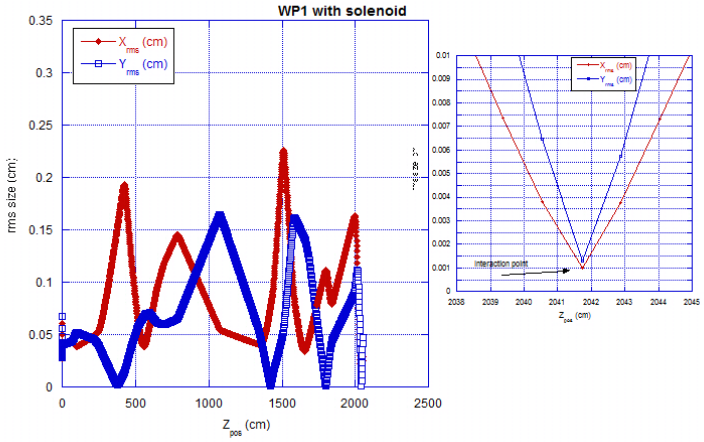

Figure 21: *Evolution of the rms electron beam sizes along the trasnfer line (left) and at the interaction point (right) for the same WP1 with the solenoid magnet focusing.*

2. S. Bellucci S. Bellucci, S. Bini, M. Castellano, A. Clozza, L. Cultrera, G. Di Pirro, A. Drago, M. Esposito, M. Ferrario, D. Filippetto, A. Gallo, G. Gatti, P. Gaudio, A. Ghigo, G. Giannini, A. La Monaca, T. Levato, F. Micciulla, M. Migliorati, D. Nanni, E. Pace, L. Palumbo, A. Petrucci, M. Richetta, C. Sanelli, A. Tenore, F. Terra, S. Tomassini, C. Vaccarezza, C. Vicario, C. Benedetti, G. Turchetti, A. L. Bacci, F. Broggi, M.M. Cola, A. Flacco, C. Maroli, M. Passoni, V. Petrillo, N. Piovella, R. Pozzoli, M. Rom?e, A. R. Rossi, L. Serafini, D. Batani, R. Benocci, C.A.Cecchetti, A.Gamucci, D.Giulietti, L.A.Gizzi, L.Labate, N.Pathak, F. Piastra, N. Drenska, R. Faccini, P. Valente, NTA PlasmonX, on "Annual Activity Report 2009", (2010).

3. L. A. Gizzi, E. Clark, D. Neely, L. Roso, and M. Tolley, High repetition rate laser systems: targets, diagnostics and radiation protection, AIP Conf. Proc. The 2nd International Conference on UltraIntense Laser Interaction Science, Vol. 1209, pp. 134-143, February 2, 2010 doi:10.1063/1.3326308

4. F. Anelli, A. Bacci, D. Batani, M. Bellaveglia, C. Benedetti, R. Benocci, L. Cacciotti, C.A Cecchetti, O. Ciricosta, A. Clozza, L. Cultrera, G.Di Pirro, N. Drenska, R. Faccini, M. Ferrario, D. Filippetto, S.Fioravanti, A. Gallo, A. Gamucci, G. Gatti, A. Ghigo, A. Giulietti, D. Giulietti, L. A. Gizzi, P. Koester, L. Labate, T. Levato, V. Lollo, E. Pace, N. Pathack, A.R. Rossi, L. Serafini, G. Turchetti, C. Vaccarezza, P. Valente, C. Vicario, *Design of the Test Experiment for the Sub-Petawatt Flame Laser System at LNF-Frascati: Electron Acceleration with Self-Injection (SITE)*, Unpublished, October 2009.

5. L. A. Gizzi, C. Benedetti, S. Betti, C. A. Cecchetti, A. Gamucci, A. Giuliettia, D. Giulietti, P. Koester, L. Labate, T. Levato, F. Michienzi, N. Pathak, A. Sgattoni, G. Turchetti and F. Vittori, Laser-Plasma Acceleration: First Experimental Results from the Plasmon-X Project, Proceedings of the 51st Workshop of the CHANNELING 2008 Conference on "Charged and Neutral Particles Channeling Phenomena", World Scientific Publishing, The Science and Culture Series - Physics, pp. 495-501 – Published April 2010, ISBN:978-981-4307-00-0.

6. L.A.Gizzi, T. Levato, L.Labate, C.A.Cecchetti, N.Drenska, R.Faccini, D. Giulietti, S.Martellotti, N.Pathak, F. Piastra, P. Valente, Abstract, Plasma Physics Conference, European Physical Society, 2011

7. M. Galimberti, A. Giulietti, D. Giulietti, L.A. Gizzi, Rev. Sci. Instrum. 76, 053303 (2005)

8. R. Faccini, F. Anelli, A. Bacci, D. Batani,M. bellaveglia, R. Benocci, C. benedetti, L. Cacciotti, C.A. Cecchetti, A. Clozza, L. Cultrera, G. Di Pirro, N. Drenska, M. Ferrario, D. Filippetto, S. Fioravanti, A. Gallo A. Gamucci, G. gatti, A. Ghigo, A. Giulietti, D. Giulietti, L.A.Gizzi, P. Koester, L. Labate, T. Levato, V. Lollo, P. Londrillo, S. Martellotti, E. Pace, N. Patack, A. Rossi, F. Tani, L. Serafini, G. Turchetti, C. Vaccarezza, P. Valente, Multi-GeV electron spectrometer, Nucl. Instrum. Meth. Phys. Res, A 623, 704-708 (2010).

9. M. Ferrario *et al* ICFA Beam Dyn. Newslett. 46 49-58, 2008

10. P. Oliva et al., Nucl. Instrum. Meth. A 615 93-99, (2010)

11. A. Bacci et al, Nucl. Instrum. Meth. A 608 S90-S93, (2009)

12. U. Bottigli, et al., IL NUOVO CIMENTO, **29C**, N.2 , MarzoAprile 2006.

13. W.J. Brown, et al., Phys. Rev. STAB **7** (2004) 060702

14. D. Alesini, et al., Nucl. Instr. and Meth. A **586** (2008) 133.